Trajectory, fate, and magnitude of continental microplastic loads to the inner shelf: A case study of the world's largest coastal shallow lagoon

Carolina Rodriguez, Pablo Silva, Laura Moreira, Larissa Zacher, Andreia Fernandes, Remi Bouyssou, Isabel Jalon Rojas, Osmar Moller, Felipe Garcia-Rodriguez, Grasiela Lopes Leães Pinho, et al.

Trajectory, fate, and magnitude of continental microplastic loads to the inner shelf: A case study of the world's largest coastal shallow lagoon.

Carolina Rodriguez [a*], Pablo Silva [a], Laura Moreira [a], Larissa Zacher [b], Andreia Fernandes [b], Remi Bouyssou [c], Isabel Jalón-Rojas [d], Osmar Moller [a], Felipe Garcia-Rodriguez [a,e], Grasiela Lopes Leães Pinho [a], Elisa Fernandes [a].

[a] Instituto de Oceanografia, Universidade Federal do Rio Grande (FURG), Rio Grande, RS, 96203-900, Brazil.

[b] Instituto de Química, Universidade Federal do Rio Grande do Sul (UFRGS), Porto Alegre 91501-970, Brazil.

[c] INRAE, 50 avenue de Verdun, 33612 CESTAS, cedex, France.

[d] Univ. Bordeaux, CNRS, Bordeaux INP, EPOC, UMR 5805, F-33600 Pessac, France.

[e] Centro Universitario Regional del Este (CURE), Ruta 9 intersección Ruta 15, Rocha, Uruguay.

∗ Corresponding author: Instituto de Oceanografia, Universidade Federal do Rio Grande, Rio Grande, RS, 96203-900, Brazil. E-mail address: carolinarp@fcien.edu.uy (C.R.).

Key Words: Coastal Plume; South Atlantic; Numerical Modelling; Plastic Fiber Transport; Accumulation Hotspots.

Abstract

The Patos Lagoon estuary is a highly significant ecosystem where freshwater from a vast and densely populated area continuously flows into the Atlantic Ocean by coastal plumes, exporting not only freshwater but also sediment, nutrients, plastics, and other contaminants. In this work, numerical modeling tools together with field data were used to assess for the first time the capacity of the coastal plume to export microplastics (MPs) to the inner shelf under different hydrodynamic conditions. Two field surveys were conducted during plume events to quantify MP concentrations and validate the model approach. A bottom-up approach was employed to estimate the potential MP export from the estuary´s domain to the Atlantic Ocean. MP concentration in surface plume waters ranged from 0.20 items m^{-3} to 1.37 items m^{-3}, confirmed by FTIR as synthetic polymers in a 90%, being Polypropylene (PP) and Polyethylene (PE) the most abundant in a 73%. The accumulation pattern was observed on the plume´s frontal system, consistent with simulation results. The estimated average MP potential export rate attained 9.0 million items day^{-1} during moderate plume events and 47.5 million items day^{-1} during high

discharge plume events. Strong discharge events, coupled with intense northeast winds, facilitated rapid southwestward export of MPs. Conversely, moderate to weak discharge events retained MPs closer to the estuary's mouth, enabling either longer trajectories or earlier deposition. Significant MP accumulation hotspots were identified in the gyre between the jetties and Cassino beach, as well as in the saline front within the plume boundaries. These accumulation zones may function as reservoirs for MP particles, potentially posing threats to local ecosystems. Understanding these dynamics is crucial for ongoing monitoring efforts to assess potential harmful interactions over time.

1. Introduction

Understanding the dispersion of plastic waste from the continent to the ocean, considering the physicochemical environmental variables, is one of the foremost current scientific challenges (Alfonso et al., 2021). Estimating MP fluxes has been one of the most pursued but still unattained objectives in this research field (Jambeck et al., 2015). It is estimated that inadequate management of plastic waste in continental areas contributes from 4 to $12x10^6$ metric tons yr^{-1}(MT) of plastics to the ocean, varying as a function of the development index of each country (Alfonso et al., 2021). Brazil, ranking fourth globally in plastic waste generation, produces $11.3x10^6$ MT yr^{-1} (equivalent to 1 kg per person per week), with only 1.28% ($145x10^3$ MT) effectively recycled and reintroduced into the production chain (Zamora et al., 2020). Mismanaged plastic waste ends up in landfills and open dumps, from where it can be primarily transported to larger water bodies through freshwater discharge and wind (Lozoya et al., 2015; Alencar et al., 2023), with rivers contributing to 80% of the total marine waste (Meijer et al., 2021). This implies that the emission probability of a country depends on its coastal extension and precipitation regime, with Brazil being responsible for around 37,799 MT yr^{-1} of plastic waste leakage into the ocean (Meijer et al., 2021).

Patos Lagoon, the world's largest coastal lagoon located in the Southwestern Atlantic Ocean (SWAO), is considered the sixth hotspot of plastic leakage to the ocean in South America, only after La Plata River, Guanabara Bay, Amazon, São Francisco, and Tocantins Rivers (Alencar et al., 2023). As part of the Southeast South America (SESA) region, Patos Lagoon is subject to the impact of El Niño-Southern Oscillation (ENSO) (Bjerknes, 1969), increasing precipitation and affecting sea level, wind, and wave patterns

(Barreiro, 2010; Schossler et al., 2018; Bitencourt et al., 2020b; Rehbein & Ambrizzi, 2022). Previous studies have demonstrated a positive impact of ENSO on continental discharge in the Northern part of the lagoon associated with an increase in pressure gradient between the estuary and the ocean, thus favoring plume formation (Távora et al., 2019). However, in the current challenging scenario of global marine plastic pollution, the impacts of different intensities of ENSO on plastics export and distribution still remain surprisingly unexplored (Morishige et al., 2007; Doyle and Gilfillan, 2016). Earlier investigations have demonstrated that extreme events and rainfall seasons over river basins are related to stronger MP transport and mobilization (Bertoldi et al., 2021; Emmerik et al., 2023a, b; Lima et al., 2023). In this context, continental discharges into the SWAO during such extreme events account for 7% of the Patos Lagoon's total volume, resulting in plumes with areas of up to 1,500 km² extending up to 50 km off the estuary mouth (Fernandes et al., 2002) under a microtidal regime and dominance of NE-SW winds (22% and 12%, respectively), where river discharge displays not only seasonal and interannual variability (Moller et al., 2001, Távora et al., 2019; Bitencourt et al., 2020a) but also interdecadal variability (Bortolin et al., 2022). Therefore, a combination of local and non-local factors governs the dynamics of the coastal plume (Marques et al., 2010b; Jung et al., 2020).

While the study of plastic contamination in aquatic environments has received numerous global scientific contributions (e.g., Abalansa et al., 2020; Alfonso et al., 2021, and references therein), comprehensive and multidimensional studies in the SWAO are limited (Rodríguez et al., 2020; Pazos et al., 2021; Pinheiro et al., 2021; Lacerda et al., 2022; Schicchi et al., 2024). According to dos Santos (2023), Patos Lagoon received plastic waste inputs ranging from 21,670 MT to 107,190 MT yr^{-1} (equivalent to 6.54 to 32.35 g day^{-1} per person) between 2010 and 2017, composed of polyethylene (PE), polypropylene (PP), and polyvinyl chloride (PVC) as the main polymers. Alves et al. (2022) identified MPs (mainly fibers) as chronological markers in sediment cores within the Patos Lagoon estuary and Mirim Lagoon (**Fig. 1**), with the first appearance dating back to 1970 CE. This finding highlights the impact of the Anthropocene and industrial activities on the local sedimentary history. Recent studies have also identified MPs in oceanic waters in South Brazil, where the highest concentrations of MPs in surface water at two Rio Grande do Sul stations, near the coastal plume influence area (Lacerda et al., 2022). In this context, the Patos Lagoon is potentially crucial as both a source and sink of

anthropogenic waste, and ulterior export to the coastal region, make the estuary a "hotspot" of marine pollution (Pazos et al., 2021).

Continental plastic loads, together with direct plastic inputs from fisheries, offshore industries, and other maritime activities (Boucher and Friot, 2017; Boucher et al., 2020), undergo various physical, chemical, and biological degradation processes driven by external environmental factors, such as mechanical action from wind and waves, solar radiation, oxygen availability and interaction with organisms. These processes lead to the formation of smaller size categories and dynamic changes in particle properties over time (Verma et al., 2016; Chamas et al., 2020). Consequently, estuaries are key compartments for both dispersion and fragmentation of macroplastics (>25 mm) into mesoplastics (5 mm – 25 mm) and MPs (1 µm - 5 mm), experiencing changes in dimensions and densities and altering their buoyancy properties (Jalón-Rojas et al., 2019). These characteristics distinguish them from fine sediment particles, thus justifying the need for specific analytical tools to understand their behavior and transport trends in different marine compartments (Jalón-Rojas et al., 2019).

Numerical modeling has proven to be an essential tool for studying the behavior and dispersion of MPs in marine environments, because of the need for specific approaches due to the unique characteristics of MPs compared to suspended sediment particles (Critchell and Lambrechts, 2016; Jalón-Rojas et al., 2019). Current numerical modeling tools, complemented with field validation, offer a low-cost methodology with high spatial and temporal resolution and integration of both experimental and field data to achieve high model accuracy (Hardesty et al., 2017). Hybrid models combining hydrodynamics with Lagrangian process-based approaches and statistical data have been widely used to predict areas of high MP accumulation (Uzun et al., 2022). In this regard, the TrackMPD model, developed by Jalón-Rojas et al. (2019) as an extended Lagrangian-based open-source tool, integrates hydrodynamic models and real-world process equations for tracking plastic particles in natural environments (Jalón-Rojas et al., 2019). TrackMPD applications have been worldwide demonstrated in recent years in various coastal and estuarine environments (Cheng et al., 2020; Baudena et al., 2022; 2023; Liao et al., 2023; Kim et al., 2023; Schicchi et al., 2023).

In this sense, this approach was performed with the objective of understanding the role of coastal plumes in the dispersion dynamics of MPs in inner shelf ecosystems, to test the hypothesis that different discharge intensities would determine different patterns

in the magnitude of export, distribution and fate of MPs to the SWAO. The transport of MPs was assessed for weak (2014-2015) and very strong (2015-2016) El Niño intensities to identify different "hotspots" of MP accumulation in the export region as a function of plume intensity. Two field sampling surveys validated the model and provided the basis for estimating MP export flux, thus elucidating the coastal plume role in the dispersion of continental MP export to the SWAO.

2. Methods

2.1. Study area

Patos Lagoon (30-32ºS; 50-52ºW, **Fig. 1**) is the world's largest choked coastal lagoon (Kjerfve, 1986), with an area of 10,360 km², a maximum length of 240 km, and a mean depth of 5 m. Draining a watershed of approximately 200,000 km², it is connected to the SWAO through a long and narrow channel (700 m wide at the mouth) delimited by a pair of 4 km long jetties (**Fig.1c**, Franzen et al., 2022). The channel's dredged portion, designed for navigation purposes, maintains depths varying from 16 to 20 m. The lagoon receives continental inputs from very turbid tributaries, i.e., Guaíba and Camaquã River, and São Gonçalo Channel (connection with Mirim Lagoon, **Fig. 1**). These tributaries together yield an average annual discharge of 2,400 m^3 s^{-1}, carrying a significant contribution of suspended sediments of approximately $5.1x10^6$ t yr^{-1} (Jung et al., 2020). Guaíba River is the main tributary, accounting for approximately half of the fluvial discharge into the lagoon (average flow of 1,253 m^3 s^{-1}) and carrying mean annual discharges of 2.99×10^6 ton yr^{-1} of suspended sediments from a sub-drainage basin of about 84,763 km^2. Camaquã River contributes 0.24×10^6 ton yr^{-1}, and drains a basin of about 21,657 km^2, while São Gonçalo Channel contributes 1.88×10^6 ton yr-¹ (Jung et al., 2020) from a basin area of 28.499 km^2. Extreme discharge events from the tributaries over the north region of the system are related to the inter-annual variability driven by ENSO oscillations (Távora et al., 2020, Bortolin et al, 2022).

The residence time of particles within the system was calculated at approximately 1.5 yr (for an average discharge of 1,000 m^3 s^{-1}, Moller et al., 1996), and was estimated at 68 days for maximum discharges (10,000 m^3 s^{-1}, Fernandes et al., 2002), showing a decrease inversely related to river discharge. The concentration of suspended solids decreases from the Northern end of the lagoon (38 g m^{-3}) to the Southern end in the estuarine area (10 g m^{-3}), which highlights the retention and filtration capacity of the lagoon. Mud depocenters

form in the central silty zones where current velocities are smaller than 0.1 m s^{-1} and depth is higher than 5 m (Bortolin et al., 2022). Littoral sandy zones are dominated by sediment resuspension when current velocities are higher than 0.2 m s^{-1} and depth is lower than 5 m.

The wind regime is mainly determined by NE wind (22%) interrupted by the passage of frontal systems from SW (12%) in time intervals of 3 – 16 days (Moller et al., 2001). Under conditions of high discharge (i.e., > 3,000 m^3 s^{-1}) combined with NE winds, hypopycnic plumes holding strong salinity stratification off the lagoon's mouth are observed as less dense freshwater from the river discharge flows over the denser saline water (Calliari et al., 2009). The formation of the continental discharge plume over the SWAO carries a suspended sediment concentration of up to 12 g m^{-3} (Jung et al., 2020). The Patos Lagoon coastal plume is a small-scale plume that exhibits surface variability resulting from two principal modes. The first one, associated with the southwest and southeast plume displacement, forced by northeasterly winds, accounts for 70% of the plume variability, the upward velocities in the near field, the stratification processes, and potential energy anomalies (Marques et al., 2009, 2010a). The second one, related to the north and east plume migration due to south quadrant wind during the passage of frontal systems, accounts for the remaining 19% of coastal variability, promoting downward velocities and mixing conditions in the near field (Marques et al., 2010a).

Tides display a mean range of 0.3 m and characterize the lagoon as microtidal, mainly of diurnal regime (Moller et al., 2001). Tidal effects and Earth rotation play a secondary role in the plume behavior, mainly affecting its shape, mixing process, and offshore penetration (Monteiro et al., 2011). Additionally, bed friction impacts mainly the alongshore direction in the coastal region (Marques et al., 2010b). In this sense, the advection and deformation of the dominant density fields control the mixing and stratification of the Patos Lagoon coastal plume, considering time scales associated with the influences of winds (5- and 15-day processes) and river discharge (30-day processes) (Marques et al., 2009).

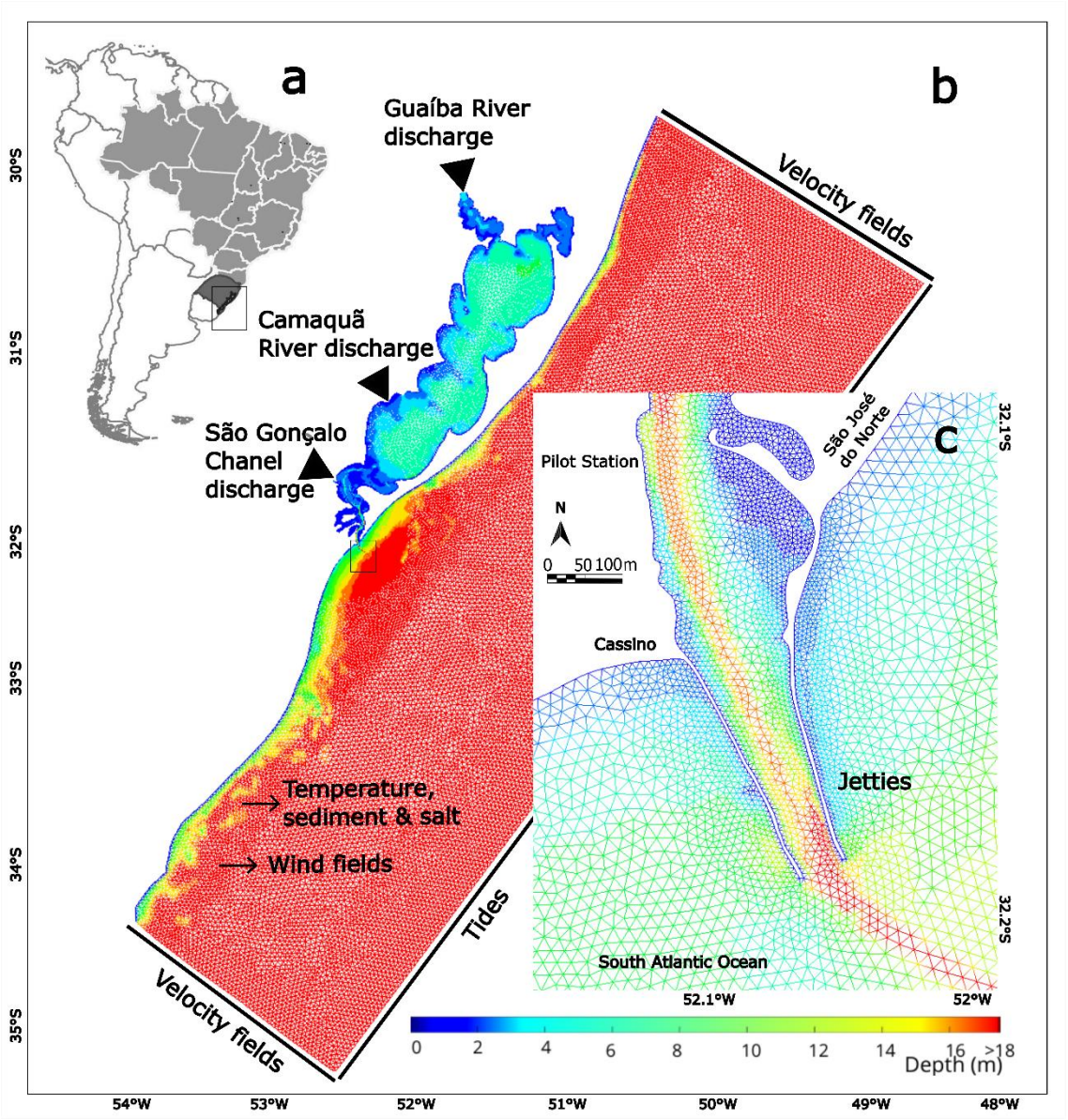

Fig. 1*. Patos Lagoon (a) bathymetry for the numerical domain and numerical mesh (b) for the simulations, where the main tributaries, i.e., Guaíba River, Camaquã River, and São Gonçalo Channel are indicated. Boundary conditions used to force the model are depicted with black solid lines. The location of the jetties (c) represents the connection with the SWAO and the area of strongest influence of the coastal plume of suspended sediments and organic/inorganic debris.*

2.2. Hydrodynamic modeling

The TELEMAC-3D model (www.opentelemac.org) has been widely employed to study the dynamics of Patos Lagoon itself (Fernandes et al., 2002), its estuary (Fernandes et al., 2004) and the resulting coastal plume (Marques et al. 2009; 2010a; Monteiro et al. 2011, Fernandes et al, 2021). TELEMAC-3D solves the 3D Reynolds-Averaged Navier-

Stokes Equations, considering the Boussinesq and Hydrostatic approximations, based on the Characteristics Method and Finite Element Method (Hervouet, 2007; Villaret et al., 2013). The TELEMAC-3D model also solves the mass conservation equation, which simulates the temporal and spatial variation of active tracers such as salinity, temperature, and suspended sediments, incorporating the flocculation process. The model domain was discretized with an unstructured finite element mesh according to Fernandes et al. (2021) (**Fig. 1b**), based on digitalized nautical charts of bathymetric data obtained from the Brazilian Navy and complementary data provided by the Rio Grande Port Authority (Portos RS). The domain covers from 29◦ and 36◦S to 48◦ and 54◦W (**Fig. 1b**) and reaches the 3700 m depth isobath. The numerical mesh consists of approximately 33,000 elements, 50,000 nodes, and seven sigma levels in the vertical, with results output every 6 h.

For the oceanic boundary conditions (**Fig. 1b**), sea level data and regional tidal velocity fields were obtained from the OSU Tidal Inversion System (OTIS – Egbert and Erofeeva, 2002), an internal coupling to TELEMAC (TPXO). Temperature and salinity fields were derived from the HYCOM + NCODA Global project (Hybrid Coordinate Ocean Model, https://hycom.org/), with a temporal and spatial resolution of 3 h and 0.08º, respectively. At the surface boundary, data from ECMWF ERA-Interim and ERA5 (European Centre for Medium-Range Weather Forecast, http://www.ecmwf.int/) were applied with a temporal and spatial resolution of 6 h and 0.75º, respectively. All these data were interpolated in time and space for each numerical grid point. Daily river discharge data from the main tributaries (Guaíba and Camaquã) provided by the National Water Agency (ANA, www.hidroweb.ana.gov.br) were used for continental boundaries. Discharge data for the São Gonçalo Channel were obtained as water level data from the Mirim Lagoon Agency (ALM, https://wp.ufpel.edu.br/alm/), and transformed into flow data using the Rating Curve Method (Oliveira et al., 2015).

The hydrodynamic output of TELEMAC was calibrated and validated for the study region by several authors (Fernandes et al., 2001, 2002, 2005, 2007; Marques et al., 2010a; Bitencourt et al, 2020a; Lisboa et al., 2022), always yielding from good to excellent values of both RMSE and RMAE. The detailed calibration and validation of the numerical mesh used in this study have already been published in Fernandes et al. (2021).

Time series of current velocities, salinity, wind intensity, and direction were extracted for the jetties area at 6 h resolution to feed discussion of the microplastic transport model

results. In this sense, the mean position of the salinity field was analyzed and used to calculate each plume duration, together with the cross-sectional vertical profile of the mean dispersion of the plumes. Pearson correlation tests were performed to evaluate the relationship between these variables in the plume's behavior, followed by linear regression to infer the type of such relationship.

2.3. Microplastic transport modeling

The TrackMPD model (Jalón-Rojas et al., 2019) simulates MP transport. TrackMPD consists of a 3D, extended Lagrangian numerical model developed in Matlab as an ad hoc open-access source to analyze the transport of plastic waste in marine and coastal systems. The model interpolates the hydrodynamic unstructured mesh from TELEMAC-3D to produce a structured mesh. To achieve a good resolution at the area of interest (i.e., jetties, **Fig. 1c**) without compromising computational time, the domain size was reduced, covering the sub-space between 52.38°-51.63°W and 32.89°-31.81°S, with a subsequent differential refinement for a better definition on the jetty's region.

TrackMPD differs from traditional Lagrangian particle tracking models by modifying particle characteristics over time and attributing specific behaviors. It consists of interactive and independent modules, which make it possible to incorporate all physical processes (such as advection, vertical and horizontal dispersion, sinking, resuspension, stranding, washing-off, and wind transport) together with the physical properties of the materials (size, density, and shape) and their behaviors (e.g., degradation and biofouling, modifying the above characteristics in the indicated time frame). For further details on TrackMPD calculations, readers can refer to Jalón-Rojas et al., (2019), Jalón-Rojas & Marieu (2023), and the Supplementary Data (Annex I).

2.4. Selection of simulation parameters for TrackMPD

The simulated periods were chosen based on the Ocean Niño Index (ONI) values (https://ggweather.com/enso/oni.htm). NOAA developed ONI to identify positive or negative El Niño (La Niña) events in the Tropical Pacific using the three-month average surface temperature (SST) anomaly for the Niño 3.4 region (5ºN-5ºS, 120º-170ºW). The ONI classification allows identifying the intensity of events for at least three consecutive overlapping three-month periods, between "Weak" (with an anomaly of 0.5 to 0.9 SST), "Moderate" (1.0 to 1.4), "Strong" (1.5 to 1.9) and "Very Strong" (≥ 2.0) events. In this

sense, we selected neutral (Mar/2014-Oct/2014), weak (Oct/2014-May/2015), and very strong (Aug/2015-Mar/2016) El Niño phases as simulation periods. For each period, three well-represented plumes were chosen from the salinity and current velocity field, considering a time scale from hours to a few days for each simulation, where the processes of coastal plume formation are more important. The selected periods of simulation and further statistics are provided in results section 3.3.

Sensitivity tests were conducted to identify numerical configurations that most accurately represented the simulation processes. For each parameter, activation within the control scenario (involving passive particles in the advective field provided by the TELEMAC velocity field) was carried out, with the aim of selecting values that closely resembled those of the control simulations. In this sense, vertical and horizontal dispersion coefficients were tested, together with the computational time for internal calculation and output liberation, the number of particles, and the release point. Horizontal (Kh) and vertical (Kv) dispersion coefficients were set up to typical values from coastal systems: 0.25 for Kh and 10^{-5} for Kv (Bogucki et al., 2005; Diez et al. 2008; Jalón-Rojas et al., 2019), as the small variations in these parameters didn't show significant changes. The computational time was also tested, varying from 2 sec, 30 sec, 1 min, 5 min, 10 min, and 15 min. The 10 minutes timestep was selected since it showed the best resolution in the particle's trajectories, without being as computationally expensive, as was observed for the shorter times. The particle amount was optimized by testing with 240 particles to ensure a comprehensive representation and facilitate even distribution across the available logical processors for efficient simulations. Finally, the release point was selected by initially considering the sampling sites and subsequently determining the location where the export behavior of the coastal plume through the jetties could be most effectively observed.

Because the time scale was used to focus on plume behavior, the effects of degradation and biofouling were disregarded for the simulations, and only the deposition and resuspension modules were activated. Then, for each plume event simulated, we use two configurations of TrackMPD: (1) passive scenario only with advection and dispersion (incorporating the values of the horizontal and vertical dispersion constants Kh and Kv, respectively) and (2) sinking scenario with advection, dispersion together with the deposition resuspension modules activated. **Table 1** resumes the main parameters chosen for each scenario.

The characterization of the particles was defined from one of the most represented items in field sampling (Section 3.1, **Fig. 2**) in terms of MPs type and average size, the same as referred to in other coastal and ocean environments from the literature (Zhao et al., 2019). Polyester fibers, highly produced in the industry (Geyer et al. 2017), were reported as a land source important contribution from industrial and urban washing machines, that are not being retained by effluent treatment plants (Napper and Thompson, 2016). Thus, polyester fiber was selected for the TrackMPD simulations and the reference value of density according to the type of particle was used as 1380 kg m^3 (Nguyen et al. 2022). The sinking behavior was set up by adding the constant settling velocity value (Ws) of 0.1 mm s^{-1} proposed as the lowest value experimentally found by Nguyen et al. (2022) for polyester fibers and referenced by Jalón-Rojas et al. (2021) as a relatively low value characteristic of small fibers.

Table 1. *Summary of the particle parameters such as size, polymer type, density, and settling velocity, and the configurations selected for the simulations, such as timestep for the calculations and for the outputs, dispersion constants, and particle behaviors modules selection for activation.*

GENERAL PARAMETERS								
Cores	TimeStep Calc	TimeStep Out	# days	Particle Shape	Particle Polymer	Particle Density	Particle Size	Particle Dequi
	10	10	Plume duration	Fiber	Polyester	1380*	0.0015	0.0012

TRACKMPD SIMULATION CONDITIONS								
	Kh	Kv	Initial Ws Option	Beaching	Refloating	Deposition	Resuspension	Biofouling
1. PASSIVE: (Advection + Dispersion)	0.25	10^{-5}	0	No	No	No	No	No
2. SINKING: (Advection + Dispersion + Deposition)	0.25	10^{-5}	0.1 mm s^{-1}*	No	No	Yes	Yes	No

**Nguyen et al, 2022.*

2.5. Model results postprocessing

For each simulation, total particle displacements were calculated as the resulting distance from the liberation point to the final position, and total trajectories were determined as the sum of distances covered by particles at each timestep. Statistical analysis included a one-way ANOVA with posthoc Tukey HSD analysis to assess the statistical differences in total displacement and trajectory. In addition to the ANOVA, a

linear regression, and Principal Component Analysis (PCA) were applied to reduce dimensionality and characterize the relationship between particle distances, water discharge, plume duration, and wind intensity.

The spatial distribution of MPs was represented by calculating the density probability maps for surface and vertical dispersion. For this purpose, the longitude, latitude, and depth of each particle at each time step was computed, the number of particles was quantified in the grid, and then normalized with respect to the total number of data points in the specified arrays to obtain a probability distribution in the study domain. Vertical density figures (Supplementary Data, Fig. S8, S12, among others) represent results as depth versus time probability, showing the time steps until final fate.

2.6. Model validation with field data

The transport trends of MPs were validated by undertaking two field surveys with a total of seven surface water collections within the study area in the context of the PLUMPLAS Project (Zavialov et al., 2020). MP density accumulation results were compared to TrackMPD simulations results (similar configuration to those described above) performed for the same data of field collections.

Sampling was carried out during plume formation events, corresponding to June 3rd and July 21st, 2022, using a 300 μm "Manta" type surface trawl, 30 x 60 cm mouth and 2 m long (Zheng et al., 2021). Surface layer suspended material was collected for approximately 15 min at each transect (**Fig. 3**). The in-situ measurements were synchronic with Acoustic Doppler Current Profiler (ADCP) and conductivity, temperature, and depth (CTD) readings, acquired at 0.1 m intervals. These measurements provided information on current velocity and water flow filtered by the net, along with the physical characterization of the water mass (**Table 2**) as recently recommended by Defontaine and Jalón-Rojas (2023).

Samples were stored in glass jars and taken for post-processing in the laboratory, following the methodology suggested by Zheng et al. (2021) and adapted for our case study. All steps were performed with special care to avoid environmental and systemic cross-contamination, using cotton lab coats, manipulation bell, glass materials such as Petri dishes, filtration system and containers, and metal tools such as spatulas and tweezers, all cleaned with distilled-filtered water beforehand (Bogdanowicz et al. 2021).

Samples were processed with 30 mL of 35% H_2O_2 previously filtered and digested in an oven at 40ºC for at least 48 h until organic matter was removed (Pfeiffer & Fisher 2020). Subsequently, samples were filtered in a vacuum system, inside a closed hood to avoid environmental contamination, on 95 mm nitrocellulose filters with 300 µm porosity, and stored in glass petri dishes. The dry filters were analyzed under a tri-ocular stereoscope (COLEMAN, model NSZ 606T) coupled to a camera and the Opticam Microscopy OPTHD software (version 3.7.11443.20180326) inside a closed protective hood, and items identified as potential plastic were characterized at 10x magnification according to size, shape, and color. These debris particles were chemically characterized using Fourier-transform infrared (FTIR) spectroscopy analysis (Bruker's Alpha P) in ATR mode using a zinc selenide (ZnSe) crystal in the region of 4000-600 cm^{-1} with a resolution of 4 cm^{-1} and 128 scans. The particle spectra were processed and identified using the Open Specy library (https://openanalysis.org/openspecy/) (Cowger et al., 2021) and then the total MP concentration was corrected incorporating the percentage of synthetic particles observed by the FTIR analysis.

Blanks were used to assess contamination of both the lab procedure itself and the environment (Bogdanowicz et al., 2021). In this sense, each sample was accompanied by a blank Petri dish with a clean filter throughout the procedure, which was treated the same as the samples were. To evaluate the contamination of the whole filtration system, an extra blank was performed using the same procedure as the samples, but without a sample. When plastics were detected in the blanks, the same items were finally removed from the sample and those recorded in the system blank were also removed for all samples.

The concentration results of MPs were also utilized to extrapolate the MP export rate of the upper layer of the estuary mouth, by employing a bottom-up approach (Boucher et al., 2019). This involved considering the observed surface concentration of MPs at the sampling point near the mouth of the jetties. This place corresponds to where the water flow was estimated for each survey, and where the lowest concentration of MPs was recorded. The water discharge on the upper 1 m layer was calculated by extracting the water current velocity fields from the modeling results and by multiplying them by the surface area, estimated at 700 m^2. This allowed us to calculate the total export of MPs by the surface layer of the plumes under differential conditions of water discharge, in a conservative way.

3. Results

3.1. Field data for model validation

3.1.1. Observed MPs

MPs were detected in all seven surface water samples (**Table 2**). A total of 2564 potential plastic particles were counted and identified, ranging from 93 to 725 items per transect (**Fig. 2**), with an average of 0.85 items m^{-3} (SE = 0.48 items m^{-3}). Length ranged from 0.04 to 98.97 mm, categorizing most of the particles as MPs (i.e., 1 µm - 5 mm) where the highest size frequencies were detected (92%). Mesoplastics (5 mm - 25 mm) were detected with lower abundance (8%), and finally, just a few macroplastics were observed (> 25 mm) (**Fig. 2**). Fibers represented 47% of the total MPs observed, being the rest 53% fragments (including films and spheres).

The relative percentage of polymeric composition per sampling station in each field survey is presented, as analyzed by FTIR spectroscopy is shown in Fig. 2. A total of 209 items was processed, constituting 8% of the total particles, with 189 items (90%) identified as synthetic polymers. Eight different polymeric types were identified, where Polypropylene (PP) and polyethylene (PE) accounted for 76% of confirmed plastic particles, being the most representative polymers from recovered items. In the analysis of June-MPs, polypropylene (PP) was the dominant polymer, i.e., 36%, followed by polyethylene (PE) 30%, alkyd varnish from polyester resin paints 20%, polyester (PES) 11%, and polystyrene (PS) at 2%. In July-MPs, a higher polymeric diversity was observed, especially in sampling station 1. Polyethylene was the most representative type with 55%, followed by polypropylene 24%, polystyrene 9.66%, polyester 6%, epoxy resin 2%, rubber 2%, alkyd varnish 1%, and ethylene-vinyl acetate (EVA) 1%.

Table 2. *Field sampling characteristics and MP concentration for modelling validation.*

	Station	Transect distance (m)	Filtered Volume (m^3)	Water Discharge* ($m^3\ s^{-1}$)	Plastic Fragments	Plastic Fibers	Total Plastics	Plastic concentration (items m^{-3})
June -03- 2022	1	2037	367	5900	59	114	174	0.47
	2	2408	433		102	138	239	0.55
	3	2315	417		50	33	83	0.20

July-21-2022	1	2100	378	10576	177	121	298	0.79
	2	1716	309	11472	124	107	231	0.75
	3	2554	460	11087	427	204	632	1.37
	4	2890	520	7418	283	368	652	1.25

*Water discharge through the lagoon outlet, estimated using fixed ADCP located at Pilot Station (**Fig. 1c**), multiplied by the current speed by the section area for the high level (10,000 m^2) by the flow period (estimated in 12 hours).
MP concentration was corrected according to the results of the FTIR analysis, i.e., 90% of the observed potential MPs.

Fig. 2 shows the characterization of analyzed particles for both field samplings (June 3rd to the left, July 21st to the right of the plot), where the number of items per sample (top) and the size distribution frequency (middle) are shown, together with the FTIR results (bottom). During the June 3rd field survey (**Fig. 2** - left), the mean concentration of all transects was 0.40 items m^{-3} (SE = 0.19 items m^{-3}). In the first transect, outside the jetties, a total of 174 plastic items were identified (0.47 items m^{-3}), including 114 plastic fibers (0.31 items m^{-3}) with an average length of 1.82 mm and 59 plastic fragments (0.16 items m^{-3}) with an average length of 0.52 mm. The second transect, set perpendicular to the first, yielded 239 plastic items (0.55 items m^{-3}), comprising 138 plastic fibers (0.31 items m^{-3}) with an average length of 0.19 mm, and 102 plastic fragments (0.23 items m^{-3}) with an average length of 0.55 mm. The third transect, conducted next to the jetties' mouth, showed a total of 83 potential plastic items (0.20 items m^{-3}), which consisted of 33 plastic fibers (0.08 items m^{-3}) with an average length of 5.29 mm, and 50 plastic fragments (0.12 items m^{-3}) with an average length of 2.08 mm.

During the July 21st field survey (**Fig. 2** - left), the samples attained a mean concentration of 1.04 items m^{-3} (SE = 0.31 items m^{-3}). The first transect was located next to the jetties' mouth, where a total of 298 plastic items (0.79 items m^{-3}) was observed, including 121 plastic fibers (0.32 items m^{-3}) with an average length of 5.39 mm, and 177 plastic fragments (0.47 items m^{-3}) with an average length of 1.95 mm. The second transect was conducted within the jetty's channel, resulting in a total abundance of 231 plastic particles (0.75 items m^{-3}), consisting of 107 plastic fibers (0.34 items m^{-3}) with an average length of 1.21 mm, and 124 plastic fragments (0.40 items m^{-3}) with an average length of 1.22 mm. The third transect, located outside the jetties where the plume front was observed, exhibited a total abundance of 632 items (1.37 items m^{-3}), including 204 plastic

fibers (0.44 items m^{-3}) with an average length of 2.16 mm and 427 plastic fragments (0.93 items m^{-3}) with an average length of 0.94 mm. The fourth transect, was conducted in the Pilot Station area transversely set to the channel and recorded a total abundance of 652 plastic items (1.25 items m^{-3}), consisting of 368 plastic fibers (0.71 items m^{-3}) with an average length of 3.13 mm and 283 plastic fragments (0.54 item m^{-3}) with an average length of 1.28 mm.

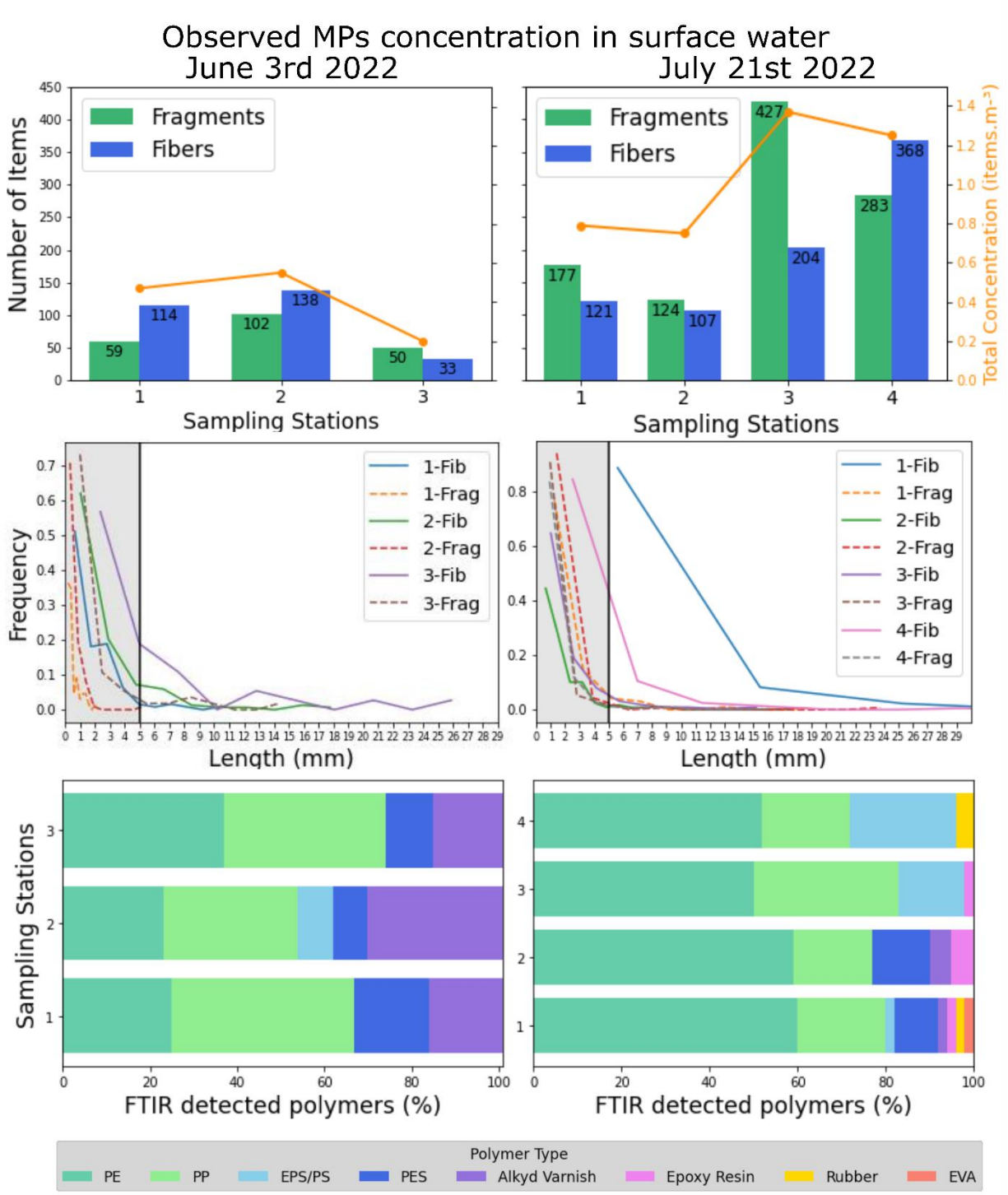

Fig. 2*. Field observed results and FTIR analysis from the manta net surface samplings for both June 3rd (left) and July 21st, 2022 (right). The uppermost plots show number of items corrected according to the results of the FTIR analysis, following the classification as fragments (green) and fibers (blue) for each sampling station, and the second Y-axis (on the right) expresses in orange line the total concentration values for each station in items.m^{-3}. Middle-plots show the length frequency distributions, where each MP category (1 µm - 5 mm) is pointed out within the vertical a gray box, where the solid lines correspond to fibers and dotted lines correspond to fragments. The lowermost plots show the relative polymeric composition of identified MPs by FTIR spectroscopy, according to the color references described below.*

3.1.2. Model validation

For model validation purposes, **Fig. 3** shows the concentration (items m^{-3}) of field-sampled MPs on the left side of the plot together with the TrackMPD simulation results displayed as a probability density map for each field survey (June 3 at the top, July 21 at the bottom) to the right of the panel. TrackMPD results revealed a good agreement between observed and simulated data. While a direct quantitative comparison of these variables is not feasible, a qualitative assessment reveals a consistent concentration pattern in both observed and simulated scenarios. Notably, both situations exhibit a similar trend of higher MPs concentration near the saline front adjacent to the jetties' mouth. This consistent replication of observed patterns strongly indicates the model's reliability for reproducing the transport features of MPs.

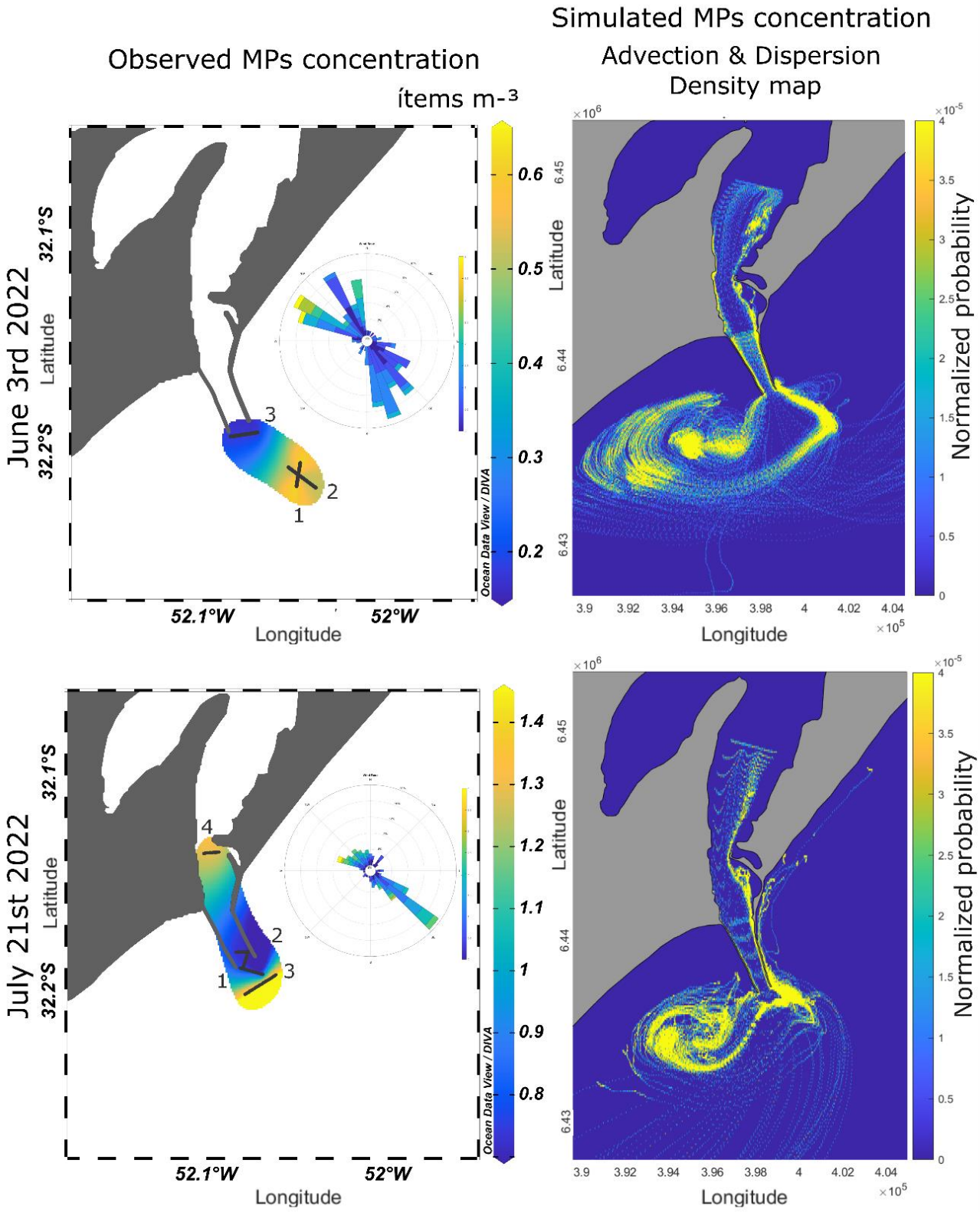

452 ***Fig. 3***. *Field experiment composition for model validation. Comparison between observed versus simulated*
453 *distribution of MPs in the coastal plume. The left section of the plot shows the spatial abundance*
454 *distribution together with the wind rose characterization, where black lines refer to the location of each*
455 *sampling station. Right plots show the TrackMPD results, simulated for the same day, expressed as a*
456 *density map. Note the similar accumulation pattern on the convergence areas of the coastal plume for both*
457 *observed and simulated data.*

458 *3.2. Estimation of MP export trough observed coastal plume events – a bottom-up*
459 *approach*

460 During the June 2022 plume event, the mean water discharge value was lower than
461 the second event of July 2022, which exhibited a strong mean discharge. The mean water
462 discharge calculated at the surface layer (1 m) represented, on average, 7% of the mean
463 water discharge out of the entire water column between the jetties on the analyzed plumes.
464 For the June 2022 survey, by extrapolating the MP concentration observed in transect 3
465 (0.20 items m^{-3}; **Fig. 2**), the water discharge restricted to the surface layer (413 m^3 s^{-1}),
466 resulted in 83 particles exported per second. This means a total export of approximately
467 7.1 x 10^6 items per day. Similarly, for the July 2022 survey, considering the MP
468 concentration in transect 2 (0.75 items m^{-3}; **Fig. 2**) and a water discharge value of 803 m^3
469 s^{-1}, the number of MPs being exported per second attained 602 items. Thus, a total export
470 of 52 x 10^6 items per day was calculated.

471 *3.3.Coastal plume hydrodynamics*

472 The time series of modeled water discharge between from the lagoon to the ocean,
473 from January 2014 to May 2016, is reported in **Fig. 4**, where positive (negative) values
474 indicate ebb (flood) flows. The mean discharge at the mouth was 2,566 m^3 s^{-1}, within
475 well-represented plume events selected based on the ONI index. Table 3 shows the
476 descriptive statistics for each of the nine simulated plumes, where the ONI condition,
477 duration, direction of deflection, and mean discharge were described. The first three
478 plumes (i.e., PL1, PL2, PL3) formed under an ENSO neutral period, the fourth, fifth and
479 sixth plume (PL4, PL5, PL6) developed under weak ENSO events, while the last three
480 plumes (PL7, PL8, PL9) formed during very strong ENSO events.

481 Results suggest that there was no significant relationship in terms of water discharge
482 at the mouth and the ONI index, but there was a significant positive relationship between
483 the water discharge and the wind intensity ($r = 0.74$; $p < 0.05$). The linear regression for
484 these variables showed a y-axis intercept value of 620.3 and the coefficient for wind
485 intensity was 1,112.7, with an R^2 of 0.54 (Fig. S4).

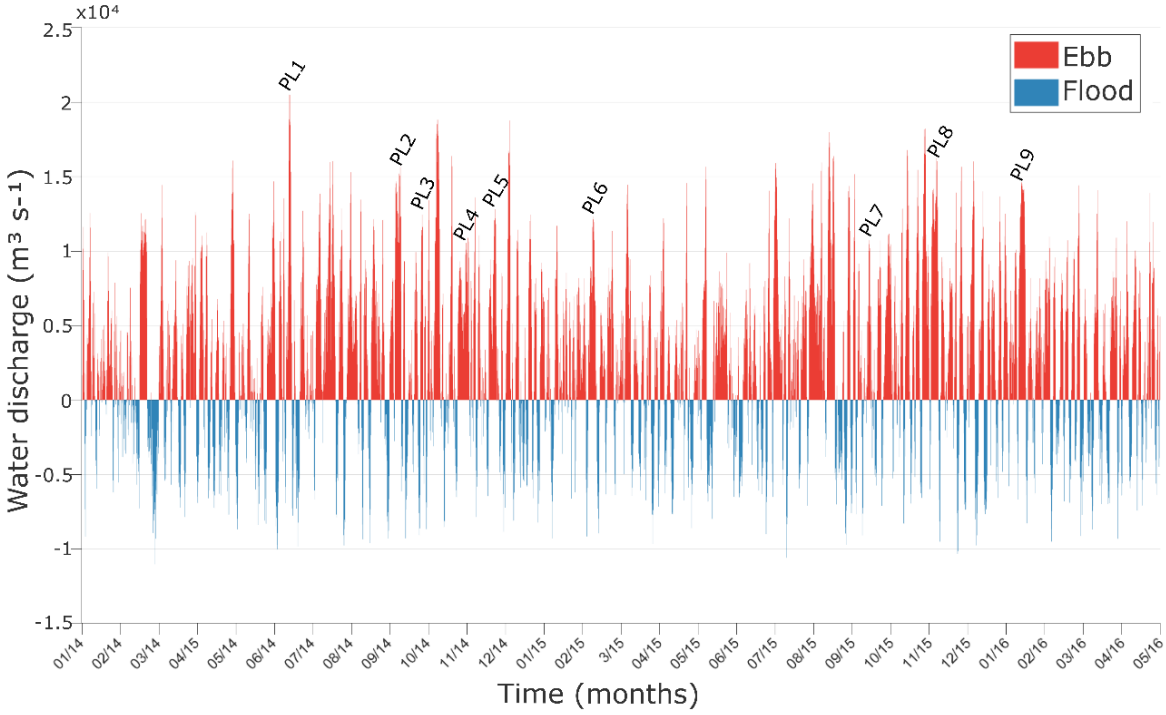

Fig. 4. *Modeled water exchange at the cross-sectional area of the jetties. Positive values refer to the discharge outflow (ebb - red), and negative values refer to the inflow (flood - blue). Each plume selected for further investigation is indicated above the discharge peaks (i.e., PL1 through PL9).*

Plumes PL1, PL3, PL8, and PL9 were classified as high-discharge events at the mouth, with mean discharge values of 10,497 $m^3 s^{-1}$, 12,555 $m^3 s^{-1}$, 12,139 $m^3 s^{-1}$, 11,167 $m^3 s^{-1}$ respectively (**Table 3**). Similarly, PL2, PL4, PL5, PL6, and PL7 were classified as either low or intermediate discharge events with mean water discharge of 6,121 $m^3 s^{-1}$, 6,956 $m^3 s^{-1}$, 6,601 $m^3 s^{-1}$, 7,439 $m^3 s^{-1}$, 6,308 $m^3 s^{-1}$, respectively. All events showed the predominance of northerly winds with different combinations of east and west wind components. Fig. 5 shows three out of the nine plumes (PL1, PL5, and PL8) to depict the common hydrodynamic trends of the plumes. The supplementary material reports the remaining plumes (Fig. S1, S2, S3).

Table. 3. Mean discharge, wind intensity, plume duration, and ONI condition for each simulated plume. High discharge events of PL1, PL3, PL8 and PL9 are depicted with bold.

REF	El Niño Condition (ONI)	PERIOD		Duration (days)	Mean Discharge ($m^3.s^{-1}$)	Mean Wind Intensity ($m.s^{-1}$)
		Initial date	Final date			
PL1	Neutral	2014/06/10	2014/06/13	3	**10,497**	8.2
PL2	Neutral	2014/07/29	2014/08/03	6	6,121	4.7

PL3	Neutral	2014/09/02	2014/09/06	5	**12,555**	10.5
PL4	Weak	2014/10/22	2014/10/29	8	6,956	5.3
PL5	Weak	2014/11/16	2014/11/22	6	6,601	6.1
PL6	Weak	2015/02/01	2015/02/06	5	7,439	8.1
PL7	Very Strong	2015/09/19	2015/09/24	5	6,308	7.9
PL8	Very Strong	2015/10/24	2015/10/31	7	**12,139**	7.7
PL9	Very Strong	2016/01/20	2016/01/25	5	**11,167**	8.3

As shown in **Fig. 5**, the onset of each plume event was observed under the sustained incidence of northeasterly winds. This wind condition modulated the water level difference between the upper and lower reaches of the estuary, thus generating the necessary barotropic pressure gradient for the freshwater export as a coastal plume to the ocean. The highest peak of discharge from the jetties' mouth (i.e., PL1), attained a maximum discharge value of 20,509 $m^3 s^{-1}$ and a mean discharge of 10,497 $m^3 s^{-1}$ during the three-day plume event. During PL5, the maximum discharge value was 12,807 $m^3 s^{-1}$ (**Fig. 4**), while the mean discharge during the six-day plume event was 6,601 $m^3 s^{-1}$. The wind incidence was predominantly from the northeast, but as the wind direction shifted to the south, the water flux was quickly reversed (**Fig. 4**), and the plume broke up and ceased to disperse freshwater to the ocean. For PL8, the maximum discharge value was 16,246 $m^3 s^{-1}$ and mean discharge of 11,167 $m^3 s^{-1}$ for the seven-day plume event.

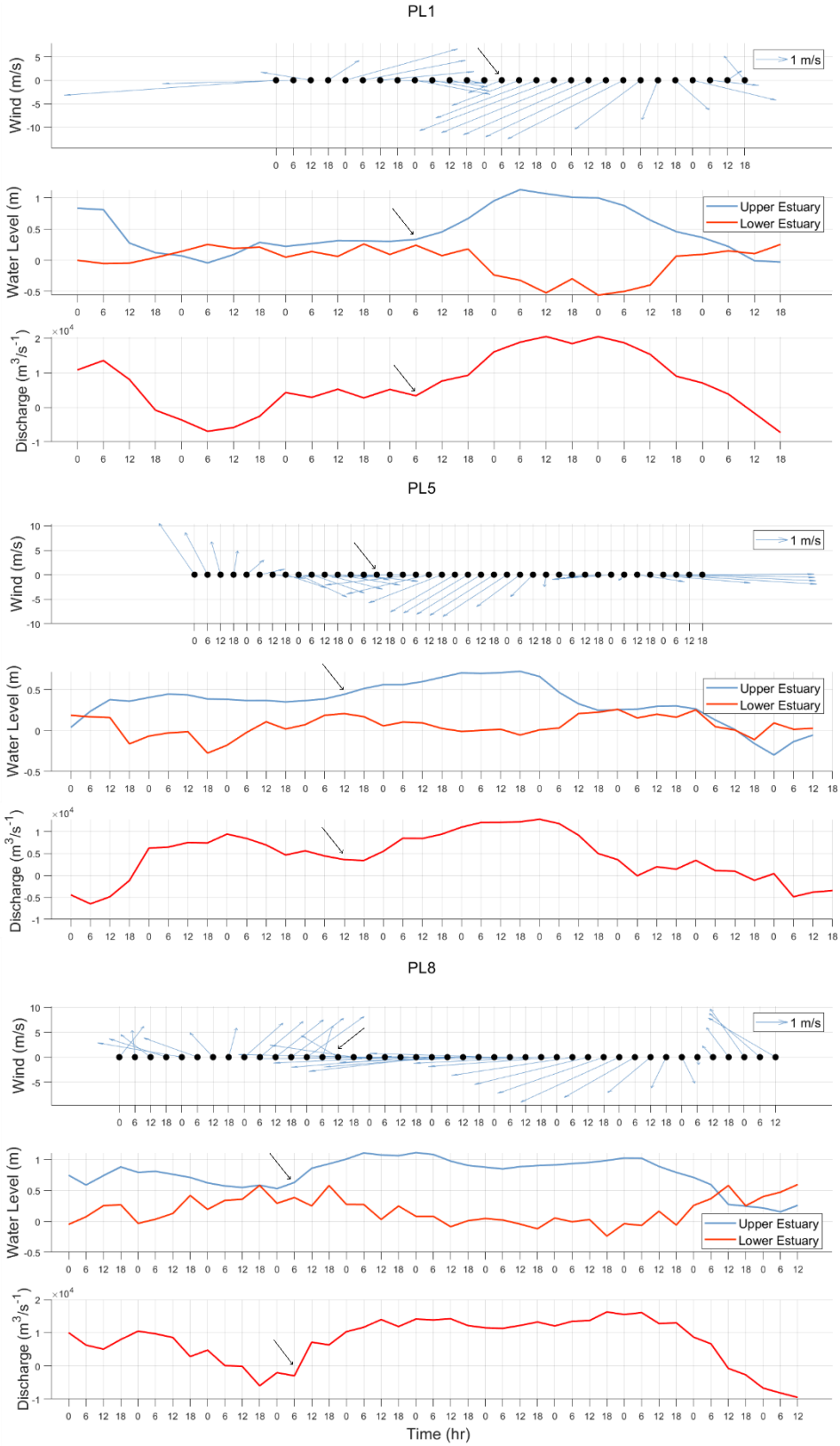

511

512 ***Fig. 5.*** *Wind intensity and direction, water level (upper and lower estuary) and water discharge at the*
513 *jetties mouth for the high discharge plumes PL1, PL5 and PL8. The time series extraction for this analysis*
514 *started three days before each plume formation. The black arrows indicate the moment of plume formation*
515 *and the time of particle release for the TRACKMPD simulations.*

3.4. MP dynamics simulations

3.4.1. Passive scenario: Advection – Dispersion simulations

The results of the first configuration are presented in **Fig. 6** as surface trajectories over the mean salinity and density maps for surface probability for all nine plumes. Such figures also show the density probability map and the wind rose characterization for a complete understanding of both MP and plume behavior. For this first set of simulations (**Fig. 6**), the particles were not only affected by advection, but also for the turbulent dispersive process. Under this configuration, the MP dynamics in the coastal plume area of influence was mainly controlled by the water discharge and wind direction.

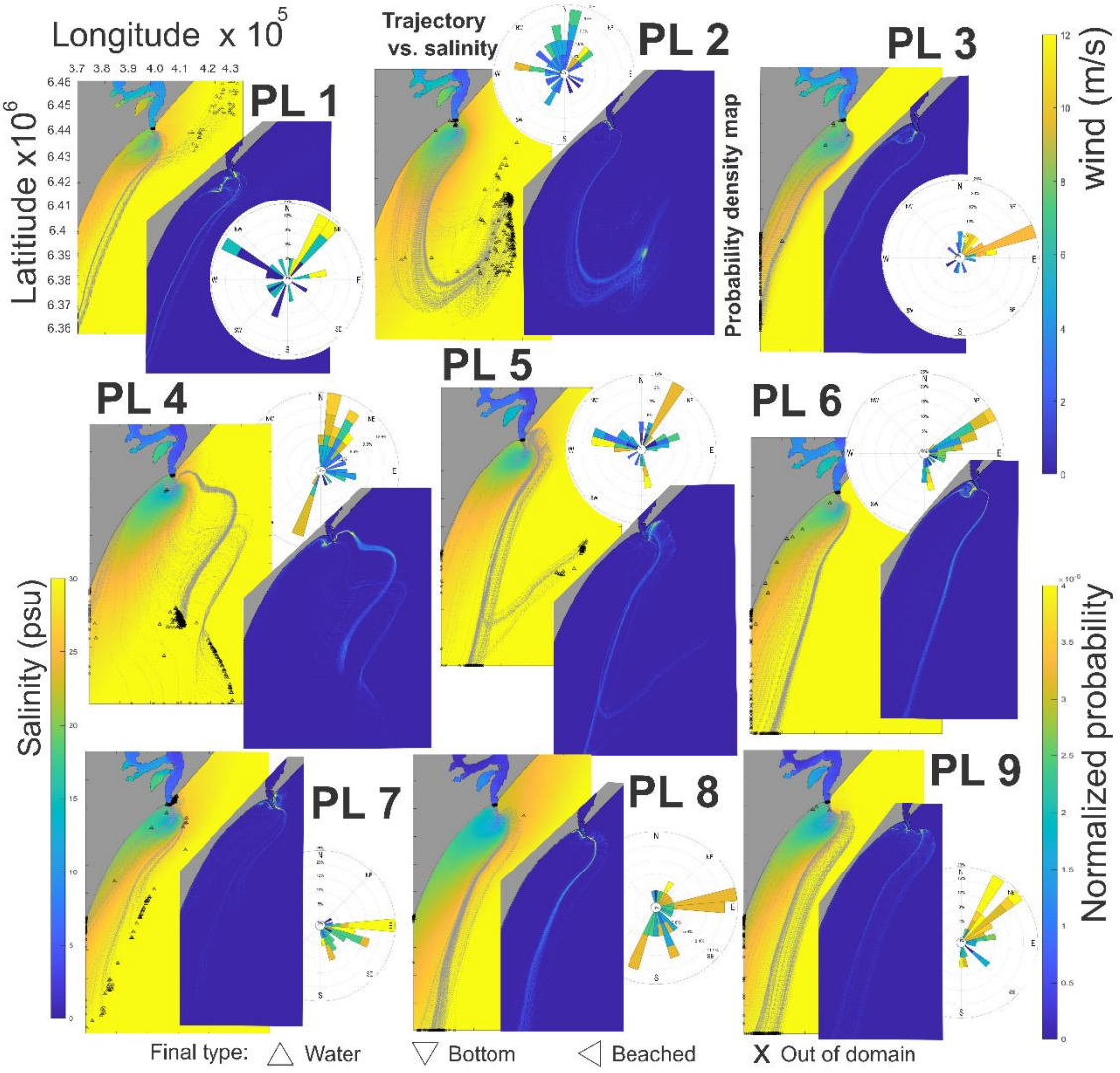

Fig. 6. *Simulated MP trajectories for advection and dispersion conditions for all nine plumes. For each plume (subplots 1-9), yellow figures are the surface 2D trajectories plotted in relation to the mean salinity, where the symbols indicate the final fate of particles, as referenced in the legend (Water▲, Bottom▼,*

Beached◄ and Out of Domain×). Blue figures show the density maps for the surface dispersion. Wind roses are also plotted for each plume to complement the understanding of the MP behavior.

As a general trend, all simulated particles of all nine plumes remained on the surface, with a south-west displacement trend, where 69% of them were transported out of the domain (Table S2), and vertically most of them reached the 5 m isobath. By the end of the simulations, particles were transported out of the domain through the south-west ocean boundary, about 49 and 86 km from the liberation point. The particle trajectories to the southwesterly direction parallel to the coastline represent the north-easterly wind response, characteristic during such plume events. When the surface trajectory was analyzed together with the mean salinity field (**Fig. 6**), particle trajectories followed the freshwater dispersion and were more likely to occur on the plume boundary, over the 25 isohalines approximately, where the saline front was located. Following this pattern, the particles accumulated rather on the small gyre generated between the west side of the jetties and Cassino beach, and on the north-easterly region of the jetties (**Fig. 6**).

Plumes events PL1, PL3, PL6, PL7, PL8 and PL9 exhibited the same accumulation pattern mainly in the gyre region and in the southwest pathway contouring the saline front about 9 km offshore. On PL1, approximately 20% of the particles showed a final fate inside the domain, and the remaining 80% was transported to the offshore region, out of domain after the 4 days of plume duration, with a tendency of accumulation in two regions. Firstly, in the gyre southwest of the jetties' mouth, and secondly along the east side of the jetties, showing first an accumulation spot in the northeast region, but then being transported to the southwest following the parallel pathway to the coastline, contouring the freshwater plume (**Fig. 6** PL1). The maximum depth attained by the particles during this event was 5 m (Fig. S8), lasting for 3 days after the liberation, but most of the particles were accumulated between the surface and 2 m depth (Fig. S9).

PL3 (**Fig. 6** PL3) had only 3% of the MP particles inside the domain at the end of the simulation, and the remaining 97% were recorded out of domain. During this 5-day event, particles showed a vertical dispersion between the 2 m depth, reaching a maximum depth of 4 m in the gyre region south of the jetties and Cassino beach (Fig. S12) after the fourth day (Fig. S13). PL6 lasted 5 days and a total of 3% of the particles remained inside the domain with the remaining 97% out of domain. Vertically, they reached a maximum depth of 6 m in the gyre accumulation spot, at the end of the simulation period (Fig. S16, S17). PL7 also lasted 5 days. The final fate of the particles showed that 60% stayed inside

563 the domain and 40% were transported out of domain by the end of the simulation. Same
564 as the behavior observed for PL1, the particles showed a dispersion firstly to the north,
565 where they first accumulated and then were transported to the southwest quadrant.
566 Vertically, the densest depth was observed between surface and 1 m depth, but the
567 maximum depth was 4 m during the second day of simulation (Fig. S20). PL8 event
568 lasted 7 days, with almost all particles transported out of the domain also in the south-
569 west boundary. The vertical distribution was on average between the surface and the 3 m
570 depth during the fourth day, with only a few particles reaching a maximum depth of 5 m
571 (Fig. S24, Fig. S25). PL9 lasted 5 days and at the end of the simulation, only 1% of
572 particles remained in the domain (and 99% out). Such a 1% consisted only of 3 particles
573 located between the jetties and Cassino beach. Most of the particles displayed a vertical
574 dispersion between the surface and 2 m depth. After the second day of simulation a depth
575 of 4 m was attained (Fig. S29).

576 PL2, PL4 and PL5 also showed MP dispersion patterns to an offshore direction. PL2
577 lasted 6 days and the expelled particles by the coastal plume were transported firstly to
578 the south-west, and then shifted to a north-east trajectory. In this case, the dispersion of
579 all the particles was completely maintained inside the domain (except for only one MP
580 particle) during the plume simulation. The densest areas were mainly located along the
581 westerly jetty outside the channel, in the saline frontline and in an offshore area to the
582 south direction. The vertical dispersion for this event was concentrated between the
583 surface and the 2 m depth, although the maximum depth in this area was 7 m at the fourth
584 day of simulation (Fig. S33). PL4 lasted 8 days and 75% of the particles remained in the
585 domain by the end of the simulation (and 25% out). The surface dispersion pattern for
586 this event showed northeasterly trajectories, where the densest regions were observed,
587 that ended up in an offshore area on the south quadrant of the domain, reaching a
588 maximum depth of 6 m (Fig. S36), after the fifth day of simulation (Fig. S37). The second
589 densest region for this event was also located in the gyre between the westerly jetty and
590 Cassino beach. PL5 consisted of a 6-day event where 17% of the MP particles stayed in
591 the domain, following an eastward trajectory, and the remaining 83% was transported
592 outside of domain by the sixth day of simulation. The densest areas were identified close
593 to the saline front to the northeast of the jetties. On the vertical axis they reached a
594 maximum depth of 4.5 m (Fig. S40), with a higher accumulation until 2 m depth, during
595 the three-day simulation (Fig. S41).

596 *3.4.2. Sinking scenario: Advection – Dispersion – Deposition simulations*

597 **Fig. 7** shows the results for the second set of simulations, where the deposition process
598 was activated as an input to the analysis of MP trajectories to represent the sinking
599 behavior in synthetic MP fiber. For all nine plumes, the main area of deposition followed
600 the freshwater dispersion with a southwest direction, parallel to the coast. Thus, 100% of
601 the particles were deposited at the bottom within the domain during the 48-hour plume
602 simulation for all the events.

603 In PL1, PL5 and PL7, two main areas of accumulation and deposition were detected,
604 the first one on the backside of the eastern jetty and the second one in the gyre region
605 between the western jetty and Cassino beach. During this dispersion pattern, particles
606 being expelled from the middle of the jetties mouth, followed first a trajectory to the east
607 and then shifted to the west during the deposition. Particles being expelled from the west
608 region, entered the gyre and deposited, whereas the remaining fraction was transported
609 southwest parallel to the coast. Particularly, plastic fibers in PL1 reached a maximum
610 depth of 13 m (Fig. S44), after 36 hours of simulation (Fig. S45). In PL5 they deposited
611 at a maximum depth of 16 m (Fig. S48) by the 48 hours of simulation (Fig. S49). PL7
612 also showed a deposition area both inside and outside the jetties' mouth, reaching 8 to 12
613 m depth, but in the southwest coastal region, the 12 m depth isobath was similarly attained
614 (Fig. S52).

615 For PL2, PL3 and PL6 there were two main areas of fiber deposition, one between
616 the jetties and Cassino beach, and the other in the southwest portion of the domain, just
617 off the freshwater boundary. The highest probability of occurrence of these MP fibers
618 under such event conditions was observed in the saline front and in the gyre. Thus, the
619 vertical trajectory plots for these events indicate that particle dynamics during the
620 deposition process, formed a loop until reaching a depth of 10 to 12 m in the gyre next to
621 the jetties in less than 24 hours. However, for PL2, the deepest deposition point was
622 recorded in the southwest portion of the domain, i.e., at 14 m depth after 30 hours of
623 simulation (Fig. S56, S57), where a maximum horizontal displacement of 61.1 km was
624 measured (Section 3.4.3, **Table 4**). Similarly, for PL3 and PL6, fibers reached a maximum

depth of 15 m in the southwest deposition area within 42 and 48 hours of simulation (Fig. S60 and Fig. S64 respectively).

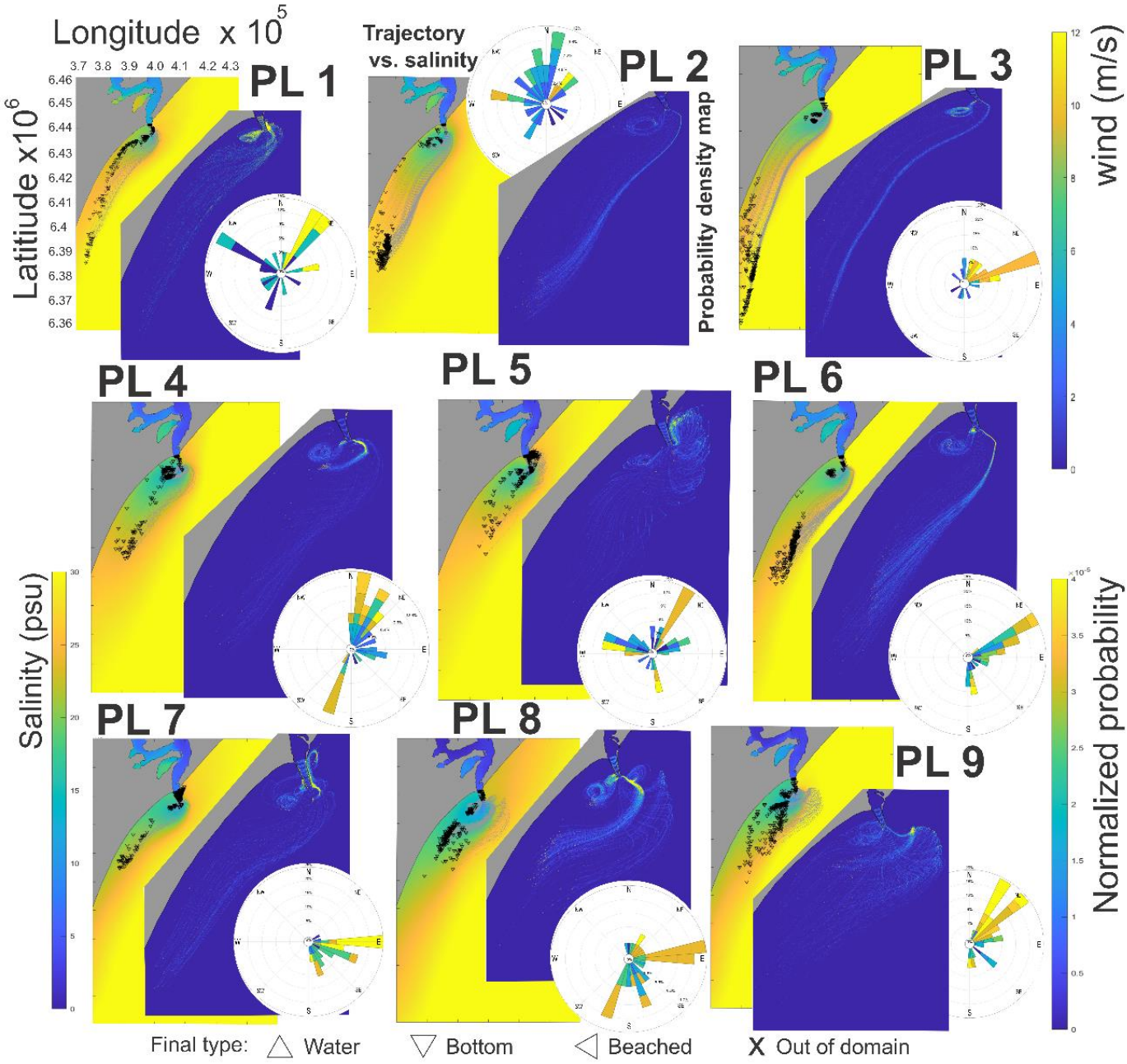

Fig. 7. *Simulated MP transport and accumulation for* PL1 *through* PL9 *considering advection, dispersion, and deposition processes. For each plume, yellow figures show the surface 2D trajectories plotted over the mean salinity, where the symbols indicate the final fate of the particles, as referenced in the legend (Water▲, Bottom▼, Beached◄ and Out of Domain×). Blue figures show the density maps for the surface dispersion. Wind rose plots are also reported for each case.*

Finally, for plumes PL4, PL8 and PL9, most of the deposition occurred in the gyre between Cassino beach and the jetties, and in the southwest coastal region, following the

freshwater dispersion. PL8 also showed deposition areas inside the jetties. Accordingly, for these simulations, the densest areas were observed within the gyre and in the eastern side of the saline front just next to the jetties' mouth. In PL4 fibers reached a maximum distance of 38.5 km away from the jetties' mouth in the southwest direction parallel to the coast. Particles attained a depth of 10 to 12 m (Fig. S68) within 24 hours of simulation, but a deepest localization of nearly 15 m was detected in the southwest coastal region within less than 40 hours of simulation (Fig. S69). In PL8, the fibers reached the 11 m depth isobath in the gyre region (Fig. S72), by the first 30 hours of simulation, whereas the maximum depth of 16 m was reached at the 48 hours of simulation (Fig. S73). In PL9, the maximum displacement distance of the fibers attained 39.6 km, and they deposited at 16 m depth (Fig. S76) within 48 hours of simulation (Fig. S77).

3.4.3. MP particles displacement and trajectories

Table 4 shows the mean, maximum and minimum horizontal displacement and trajectories traveled by the simulated MPs in the proposed scenarios, combining the nine plume events and two model configurations: (1) Passive: advection + dispersion + sinking and (2) Sinking: advection + dispersion + sinking + deposition). We observed differences in the distances attained by the particles in each plume depending on the scenario simulated and the environmental conditions forcing the MP behavior. In this sense, to understand the significance of these physical drivers, they were statistically analyzed together with the resulting distances. Under the passive configuration, the particle displacements showed a stronger positive relationship with the water discharge ($r = 0.34$; $p < 0.001$) than that of the wind intensity ($r = 0.18$; $p < 0.001$). However, when the trajectory was added to the analysis, the relationship was inverted, showing negative correlations with the wind intensity ($r = -0.48$; $p < 0.001$) and the water discharge ($r = -0.16$; $p < 0.001$). An ANOVA test showed differences in the total distance between plumes ($F = 207.1$; $p < 0.001$, Fig. S5). Also, the PCA diagram (Fig. 8), showed that the MP mean displacement was rather related to the mean discharge whereas the trajectory was related to the event duration.

Under the second configuration of sinking behavior, the displacements attained by the particles characterized as fibers, from the liberation point until bottom deposit, showed a weak positive relationship with water discharge ($r = 0.13$; $p < 0.001$), and wind intensity ($r = 0.11$; $p<0.001$). Similarly, the particle trajectories showed a low positive correlation

667 coefficient with water discharge ($r = 0.19$; $p < 0.001$), and with wind intensity ($r = 0.12$;
668 $p < 0.001$), differing from the previous scenario where this relationship was negative.

Table. 4*. Summary of the simulated surface displacement and trajectory attained by MP particles in each TrackMPD simulation.*

Plume Event	Scenario	Distance	Mean (m)	Max (m)	Min(m)	Standard Deviation
PL1	Passive	displacement	68,365	85,264	13,381	22,062
		trajectory	81,012	89,574	52,289	10,342
	Sinking	displacement	17,551	59,236	991	16,822
		trajectory	24,151	60,861	1003	15,541
PL2	Passive	displacement	38,534	60,753	316	14,080
		trajectory	109,857	131,260	21,251	24,753
	Sinking	displacement	43,562	61,098	2022	18,664
		trajectory	49,319	63,274	3260	13,371
PL3	Passive	displacement	59,372	78,629	856	13,605
		trajectory	64,995	82,272	24,645	10,743
	Sinking	displacement	43,294	83,602	1530	27,914
		trajectory	48,956	87,257	1532	25,314
PL4	Passive	displacement	56,834	83,590	5211	10,620
		trajectory	83,569	114,378	41,643	12,610
	Sinking	displacement	11,772	38,538	892	10,494
		trajectory	18,424	40,561	893	9336
PL5	Passive	displacement	73,754	85,394	20,624	16,168
		trajectory	99,724	145,827	46,594	19,678
	Sinking	displacement	5995	34,691	509	6882
		trajectory	12,905	37,666	897	6947
PL6	Passive	displacement	72,398	85,385	4115	17,272
		trajectory	79,016	87,534	37,389	11,800
	Sinking	displacement	26,021	46,697	999	14,197

		trajectory	30,997	48,905	1002	13,130
PL7	Passive	displacement	30,867	83,381	423	25,837
		trajectory	46,551	102,087	14,766	23,063
	Sinking	displacement	7001	32,193	187	9884
		trajectory	10,981	34,982	730	10,169
PL8	Passive	displacement	74,531	85,229	10,587	15,809
		trajectory	84,021	101,666	56,250	15,290
	Sinking	displacement	14,094	34,730	148	7684
		trajectory	23,806	42,026	667	10,796
PL9	Passive	displacement	73,018	85,353	3150	16943
		trajectory	80,772	98,294	17,932	16,152
	Sinking	displacement	14,295	39,622	1015	8171
		trajectory	24,158	42,542	1016	7825

A Principal Component Analysis (PCA, **Fig. 8**) explained the variability of the system in two principal dimensions. Dimension 1 accounted for nearly 50% of the variance and was interpreted as wind intensity and water discharge gradient, together with the displacement of the particles, on the left side of the axis, opposite to the plume duration and trajectory. Dimension 2 accounted for 28.5% of the total variance and was interpreted mainly as the displacement gradient. The plume events were separately grouped within the ordination diagram, where PL1, PL3, PL8 and PL9 (red dots in **Fig. 8**), were associated with higher discharge at the mouth and wind intensity. On the other hand, PL2, PL4, PL5, PL6 and PL7 (light blue triangles in **Fig. 8**) were plotted to the left of the diagram and associated to low water discharge plume event duration.

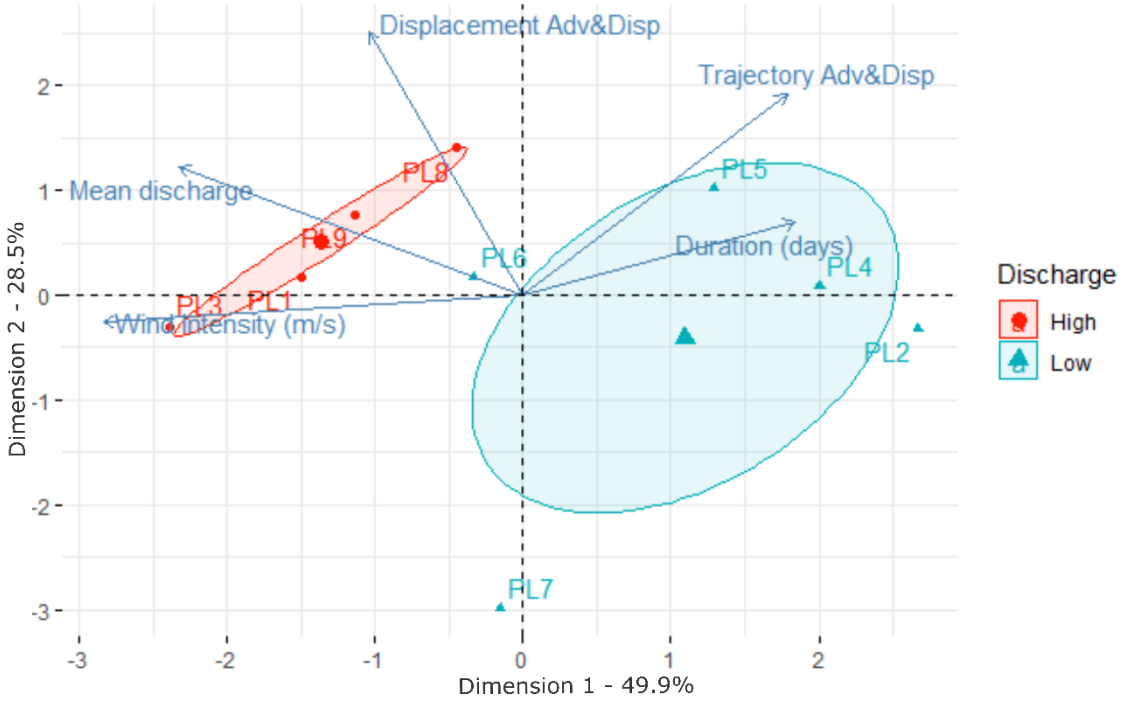

Fig. 8*. PCA diagram for the advection and dispersion scenario for all nine simulated plumes. Note that water discharge and wind intensity are negatively associated to the plume duration.*

4. Discussion

4.1. MP export of the Patos Lagoon coastal plume

4.1.1. Observed data during the model validation

This study introduces for the first-time data on the concentration of MPs exported from the plume of the world's largest choked coastal lagoon to the Southwestern Atlantic Ocean (SWAO). The magnitude of export can be considered as large values, since the lagoon hold large industrial cities and harbors. The observed accumulation patterns in the field corroborated the pattern inferred from TrackMPD simulations (**Fig. 2**). Results illustrated the tendency of the plume´s frontal system to accumulate MPs during the outward displacement from the estuary. As observed for the higher MP concentration, this pattern was observed not only in transects 1 and 2 during the June 3rd survey, but also in transect 3 during the July 21st. The higher concentration of MPs in the Pilot Station of Rio Grande, observed for transect 4 during the July 21st survey, could be related to the high traffic of daily vessels, which is also supported by the presence of paint fragments in the net samples. Fortunately, both sets validate the use of TrackMPD model for MP surface transport.

Previous investigations on the presence/abundance of MPs in this region were conducted across different natural compartments, including the salt marshes of Patos Lagoon (Pinheiro et al., 2021), Cassino Beach (Wetzel et al., 2004; de Ramos et al., 2021), and in offshore areas of the SWAO (Lacerda et al., 2022). However, because of the absence of standardization of procedures due to variations in environmental matrices, sampling methods, and reported result units, comparisons must be interpreted with caution (Pasquier et al., 2022).

According to our results, the concentration of MPs observed in surface waters of Patos Lagoon coastal plume ranged from 0.20 items m^{-3} (~59,611 items km^{-2}) to 1.37 items m^{-3} (~412,294 items km^{-2}) for all seven transects. When comparing our findings to those of Lacerda et al. (2022), where they detected 19,267 items km^{-2} in the oceanic offshore station, close to our study area, our results were approximately one order of magnitude higher because of the inherent dilution processes of the ocean. Compared to similar studies in the Guaíba River, the main lagoon tributary, Bertoldi et al. (2021) reported average concentrations ranging from 11.9 ± 0.6 to 61.2 ± 6.1 items m^{-3}, our results indicate concentrations approximately one order of magnitude lower, as Guaíba River is located very close to a large urban contamination source. This gradient in MP concentrations, from the primary tributary to the open ocean via the estuary, underscores the important role of Patos Lagoon as a buffering system prior to MP export from land to sea (Lopez et al., 2021, Meijer et al., 2021) but also de dilution oceanic process. A recent work from Queiroz et al., (2022) showed comparisons of MP abundance in surface waters of the Western Atlantic Ocean, to assess the MP fluxes from freshwater systems to open ocean in South America (Queiroz et al., 2022). Using a 64-µm mesh, they reported for the Amazon basin a mean abundance of MPs ranging from 2672 ± 1167 items m^{-3} to 4772 ± 2761 items m^{-3} during the dry and rainy seasons, respectively. Such a high abundance may be attributable not only to the basin dimension, but also to the methodology used, since almost 50% of the plastics corresponded to fractions smaller than 300 µm (the mesh size used in the present work) (Queiroz et al., 2022). Also from Brazilian waters, in the Goiana River estuary, a mean concentration of 0.26 items m^{-3} (300-µm mesh) was reported (Lima et al., 2014). In the Tamandaré Bay, Lima et al., (2023) reported a range of MP concentration of 7.8 ± 3.5 to 3.7 ± 0.6 items m^{-3} (using a 64-µm mesh plankton net), while in the Tamandaré coastal plume, the authors reported a range of 4.0 ± 0.2 to 44.6 ± 55.5 items m^{-3} during low – high rainfall respectively (Lima et al., 2023). The

FTIR polymeric characterization also showed consistency with similar regional studies where PP, and PE are the most abundant type of MPs (Rodriguez et al., 2020, Bertoldi et al., 2021). These are the most manufactured and lightest plastics, thus they are more easily found in surface water samples worldwide (Geyer et al., 2017, Zamora et al., 2020).

4.1.2. Estimation on export rate.

Table 5 shows the detailed MP export estimations calculated for all nine simulated plumes, based on this distinction according to the water discharge as identified by the PCA (**Fig. 8**). July-2022 presented a mean discharge in the same order of magnitude as the simulated plumes PL1, PL3, PL8 and PL9, grouped as high discharge events by the PCA (**Fig. 8**). By considering the estimated MP flow for both the lower and higher water discharge conditions during the June and July 2022 surveys, it would be possible to extrapolate the number of MPs being exported in each of the nine simulated plume events. As an approximate estimation, the MP export during the low-moderate water discharge simulated events ranged from 8.3 x 10^6 items day^{-1} to 10.5 x 10^6 items day^{-1} (mean: 9.0 x 10^6 items day^{-1}), while the export during the high-water discharge simulated events ranged from 42.4 x 10^6 items day^{-1} to 56.6 x 10^6 items day^{-1} (mean: 47.5 x 10^6 items day^{-1}). In this sense, the potential export magnitude of simulated plumes encompasses a wide range between 42 and 297 million of microplastic items per event.

Table 5. *Estimation of total MP export per day and per plume event based on the observed surface data obtained from the field survey and extrapolated to the mean water discharge of the surface layer and the duration of each simulated/observed plume.*

	Plume event	Duration (days)	Surface water discharge (m^3 s) *	MP flux (items day^{-1})	Total MP flux
Low discharge events	**June – 2022**	**6**	**413**	**7.1 x 10^6**	**42.8 x 10^6**
	PL2	6	519	8.9 x 10^6	53.8 x 10^6
	PL4	8	609	10.5 x 10^6	84.2 x 10^6
	PL5	6	516	8.9 x 10^6	53.5 x 10^6

	PL6	5	482	8.3×10^6	41.7×10^6
	PL7	5	491	8.5×10^6	42.5×10^6
High discharge events	**July - 2022**	**5**	**803**	**52.0×10^6**	**260×10^6**
	PL1	3	684	44.3×10^6	133×10^6
	PL3	5	717	46.4×10^6	232×10^6
	PL8	7	655	42.4×10^6	297×10^6
	PL9	5	874	56.6×10^6	283×10^6

* Calculated for the surface layer of 700 m^2

The MP export values estimated in the present study for all nine plume events were calculated as a function of the mean water discharge restricted to the surface layer. Due to the inherent water column heterogeneity, the MP concentration estimated here cannot be unfortunately extrapolated to the entire water column. The calculations were consequently limited to the surface layer, confined to of the uppermost 1 m layer. These values ranged from millions to tens of millions of plastics items being exported throughout the coastal plume. However, these values serve as an approximation to the potential MP export of the system only under these conditions. In this context, we assumed that during such discharge events, the surface layer exports MPs at comparable rate during simulations. As also pointed out by Zhao et al., (2019), the extrapolations for the MP fluxes through the estuary mouth must be therefore approached cautiously, by only recognizing them as potential exportation rate.

The estimated potential export rate of MPs revealed significant findings. On average, during low to moderate simulated plume events, the export rate was approximately 9.0 million items day^{-1}, while during high water discharge simulated plume events, it increased to 47.5 million items day^{-1}. Similarly, Zhao et al., (2019), estimated for the Changjiang Estuary (China) an export rate of 16 - 20 x 10^8 items yr^{-1} (utilizing a pump with a 60 µm size methodology). The potentially comparable values between different papers, however, are only comparable in terms of abundance instead of export rates, and

abundances were measured using different mesh size (Queiroz et al., 2022). Other recent studies on plastic riverine transport during high river flood conditions focused on the visual sorting of macroplastics for the export calculations, making it difficult to compare to our results (Emmerik et al., 2023, Lima et al., 2023). Our findings underscore the key role of coastal plumes as transport vehicles of a substantial volume of anthropogenic materials from expansive, urbanized basins to coastal and oceanic environments.

4.2. Hydrodynamic conditions

Despite the temporal co-variation between discharge tributary anomalies of the Patos Lagoon, and the ENSO phases as indicated by the ONI index (Távora et al., 2019, Bitencourt et al., 2020b), the absence of a statistical relationship between the water discharge and the ONI index can be attributed to the inherent complexity of the coastal system. Notably, during the ENSO neutral phase, we observed the most extreme discharge events throughout the jetties' mouth, which surpassed the peaks observed during both weak and very strong El Niño events. In this regard, previous studies on suspended sediment contributions from the Patos Lagoon plume demonstrated that the ENSO cycles did not significantly modify the spatial variability of inner shelf suspended sediments (Lisboa et al., 2022). This could be related to the influence of other mechanisms of ocean-atmosphere interaction exerting hierarchically more important roles than the precipitation anomalies, such as the Southern Annular Mode (SAM), associated with the ENSO phases (Schossler et al., 2018). Moreover, various authors have demonstrated that the Patos Lagoon coastal plume is primarily modulated by the wind influence at synoptic time scale, changing its direction in less than 24 h (Marques et al., 2009) in the alongshore direction (Marques et al., 2010a). In this regard, water discharge over the north portion of the lagoon is related to time scales of around 30 days (Marques et al., 2009) and plays a secondary role in the plume hydrodynamics.

The aforementioned evidence not only supports the statistical relationships between water discharge at the mouth and the wind intensity in the estuary mouth, but also corroborates that the wind influence is the main hydrodynamic modulator at this area. Similarly, PCA showed a close relationship between wind and water discharge, grouping together specific plume events under such characteristics (**Fig. 8**). We detected three groups of plumes. PL6 and PL7 were grouped in the middle section of the horizontal axis and represented events of low water discharge but high wind intensity. PL1, PL3, PL8

and PL9 represented events of high-water discharge and high wind intensity. Finally, PL2, PL4 and PL5 were characterized by low water discharge and low wind intensity. In addition to synoptic data, climate modes of variability also play an important role as northeasterly winds reported as typical for El Niño events (Marques et al., 2010a, 2011, Bitencourt et al., 2020b), which intensify the plume displacement to the southwest quadrant as observed in this study for PL1 through PL9.

4.3. Simulated MP dispersion patterns under coastal plume dynamics

4.3.1. Considerations for advection-dispersion scenarios

In response to the influence of northeasterly winds, the primary direction of particle dispersion of all plume events was towards the southwest of the domain. However, when comparing the particles displacements and trajectories between plume events for advection and dispersion scenarios, we observed differences in terms of main physical variables.

The particle displacements (trajectories) exhibited a positive (negative) correlation with water discharge and wind intensity. In plume events of high-water discharge, such as PL1, PL3, PL8, and PL9, the particles reached longer displacements quickly, traveling shorter but straight trajectories. These events showed a high percentage of particles out of the domain (80%, 98%, 100%, 99% respectively). The dispersion pattern in this group of events followed a direct southwest path, being the particles trapped in an alongshore circulation. Areas of highest particle density were observed along the coast, thus delineating the front of the saline plume, and within the gyre between the west jetties and Cassino beach. During such transport process, the particles formed a loop in this gyre. These areas of accumulation located to the south of the jetties mouth were previously reported by Marques et al. (2009; 2010b) and Fernandes et al. (2021) as recirculation zones where vertical velocities are intensified, and sediment deposition is promoted. Hence, it appears to resemble the same pattern as observed in the vertical particle trajectories where they converge downward while performing this loop, supporting the occurrence of a potential depocenter of these anthropogenic particles.

In contrast, the other group of plume events exhibited lower discharge values. Despite this fact, PL6 and PL7 also experienced strong wind intensities, resulting in particle

transport patterns comparable to those of high discharge events. Such events displayed high-density areas in the plume front and within the gyre. In the case of PL7, there was also a high-density region to the northeast behind the jetties.

On the other hand, PL2, PL4, and PL5 shared lower values of water discharge and wind intensities and displayed lower percentages of particles being transported out of domain (0%, 25%, and 83% respectively). This is evident by the longer particle trajectories during the simulation periods, performing more offshore transport patterns. In this sense, PL2 showed a hotspot of accumulation at the farthest point of the inner shelf, being susceptible to a wider redistribution by oceanic currents. Both PL5 and PL7, exhibited the accumulation pattern behind the jetties front of São José do Norte.

4.3.2. Study limitations: considerations for sinking scenarios

As the simulated vertical behavior of MPs within the plume was based in only one Ws value, there is a limitation for inferring all the MP potential scenarios in the study area considering the variability of this parameter over different water conditions and biofilm growth (Mendrik et al., 2023). Also, this validation process based on surface sampling conducted and reported also as a validation method elsewhere (Atwood et al., 2019, Gorman et al., 2020, Lopez et al., 2021), does not allow to properly validate the vertical transport of MPs. *Ad hoc* field surveys with this specific objective should be conducted to provide a comprehensive understanding of the vertical behavior of MPs on coastal plumes.

Another limitation arises from the use of a constant value of Kv, knowing that this can also change over time and space. TrackMPD can read spatio-temporal values of Kv from TELEMAC. In that case if Kv is not well estimated in TELEMAC, it can be a limitation for TrackMPD.

To enhance our understanding of this complex issue, future studies should build upon this work by exploring different periods, considering a range of climatic conditions, and examining materials with varying characteristics, including differences in density and shape. For more accurate calibration of numerical models, additional field experiments are essential to evaluate in-situ characteristics and parameters such as specific coefficients of diffusion, settling velocities and the evolution of plastic density in real estuarine conditions. Moreover, more field surveys should be conducted, specifically targeting different gradients and accumulation hotspots, and determining the MP concentration in

the whole water column. This comprehensive approach will contribute significantly to the scientific understanding of the multifaceted nature of this problem.

4.4. Ecological consequences for observed and simulated findings

The inferred patches where MPs accumulated represent areas of elevated ecological risk. These areas are characterized by the coexistence of diverse groups of organisms with both natural and human significance (Lemos et al., 2022), and they might potentially interact with the accumulated MPs.

The increased accumulation observed in the plume fronts, located between the freshwater-marine interface, is a recurring phenomenon observed for most simulations. These areas are prone to high levels of instability, driven by shearing stress (Pritchard, 2000), which triggers mixing processes contributing to the degradation and fragmentation of MPs (Wang et al., 2022). Moreover, these frontal regions are impacted by the accumulation of MPs, which can disrupt nutrient capture and biogeochemical cycles associated with frontal systems (Galgani et al., 2021; Wang et al., 2022). This suggests that numerous processes are likely increasing the bioavailability of MPs to a wide range of organisms in the food webs (Wang et al., 2022), specially during high discharge events (Lima et al., 2023). Lima et al., (2023) reported MP intense inputs from river to coastal region, during high discharge plume periods, where almost 70% of them ranged in the same size of zooplankton communities, thus demonstrating the elevated risk for zooplanctivorous organisms to ingest MPs for food (Lima et al., 2023). Supporting this, previous research in the study area has reported eight marine fish species, highly valued for commercial purposes, having ingested MPs (Neto et al., 2020). Similar findings have been documented for five species of sea turtles (Rizzi et al., 2019; Bugoni et al., 2001), procellariiform birds (Colabuono et al., 2009), fur seals (Denuncio et al., 2017; Lima et al., 2023), and sperm whales (Brentano et al., 2020). These relevant reports, together with our findings, denote the importance of this underestimated problem for the environmental quality and health of the marine ecosystem influenced by Patos Lagoon coastal plume.

5. Conclusion

The present study represents the first attempt to understand the presence, abundance, and distribution of MPs in the surface waters off Patos Lagoon estuary, which is set in a large urban conglomerate holding one of the largest harbors of Brazil. This is also the first report on coastal plume potential export rate of MPs and the dispersal mechanisms

influenced by hydrodynamics. The potential utility of the TrackMPD model as a tool for assessing and mitigating this anthropogenic pressure on the local environment under varying ambient conditions is explored. The combination of numerical modeling tools with field observations, was shown to be invaluable and cost-effective for simulating a wide range of natural conditions and identifying microplastic hotspots in the area.

The coastal plume showed surface MP concentrations ranging from 0.20 to 1.37 items m^{-3}, thus identifying this region of South America as a hot spot of transport and export of MP to the inner shelf, potentially exporting values of 9.0 - 47.5 million items day^{-1}. This conclusion is supported by the condition that the mouth of the estuary is as permanently-open system. There is a strong relationship between the discharge flow and the wind intensity as main hydrodynamic modulator for dispersion of the plume.

6. Credit authorship contribution statement

Carolina Rodriguez Perez: Conceptualization, Methodology, Formal Analysis, Investigation, Data Curation, Writing – original draft, Writing – review and editing, Visualization. **Pablo Silva**: Data Curation, Methodology, Visualization. **Laura Moreira**: Methodology. **Larissa Zacher:** Methodology. **Andreia Fernandes:** Resources, review, and editing. **Remi Bouyssou**: Methodology, Visualization. **Isabel Jalón-Rojas:** Methodology, Visualization, Resources, review, and editing. **Osmar Moller:** Methodology, Funding acquisition, Resources. **Felipe Garcia-Rodriguez:** Conceptualization, Formal analysis, Writing – review and editing, Supervision. **Grasiela Lopes Leães Pinho**: Conceptualization, Formal analysis, Resources, Writing – review and editing, Supervision. **Elisa Fernandes**: Conceptualization, Formal analysis, Resources, Writing – review and editing, Supervision

7. Funding

This study was supported by the Conselho Nacional de Desenvolvimento Científico e Tecnológico (CNPq) for C.R. master scholarship (N° 131698/2021-4), and for funding the PLUMPLAS Project: “River plumes as major mediators of marine plastic pollution.” (CNPq Grant N° 402906/2019-5).

Declaration of competing interest

935 The authors declare that they have no known competing financial interests or personal
936 relationships that could have appeared to influence the work reported in this paper.

937 **Acknowledgements**

938 We acknowledge to CNPq for the economic support of C.R. master scholarship. To
939 PLUMPLAS researchers for providing the necessary resources for the field surveys. To
940 UFRGS Chemistry Institute for the analytical facilities during the FTIR analysis. This
941 paper is a contribution to the Anthroplast Project (ONR Contract Number:
942 N629092412038). To C. Augusto Schettini for the invaluable help in analysis and
943 processing time series. To Thais Gava, Raphael Lobato, Kristhal Doto, Ana C. Soares
944 and Elis Brandão Rocha for the constant help in the analysis and discussion of this work.
945 To Lara Pinheiro, Juliana Costi and Juan Pablo Lozoya for their suggestions to improve
946 the quality of this work.

947 **Supplementary data**

948 Supplementary data to this article can be found online at ..

949 **8. References**

950

951 Abalansa, S., El Mahrad, B., Vondolia, G. K., Icely, J., & Newton, A., 2020. The Marine
952 Plastic Litter Issue: A Social-Economic Analysis. Sustainability, (1220), 8677.
953 https://doi.org/10.3390/su12208677

954 Alencar, M. V., Gimenez, B. G., Sasahara, C., Elliff, C. I., Velis, C. A., Rodrigues, L. S.,
955 Conti, L. A., Gonçalves-Dias, S. L. F., Cetrulo, T. B., Scrich, V. M., & Turra, A.,
956 2023. Advancing plastic pollution hotspotting at the subnational level: Brazil as a
957 case study in the Global South. Marine Pollution Bulletin, 194(March).
958 https://doi.org/10.1016/j.marpolbul.2023.115382

959 Alfonso, M. B., Arias, A. H., Ronda, A. C., & Piccolo, M. C., 2021. Continental
960 microplastics: Presence, features, and environmental transport pathways. In
961 Science of the Total Environment (Vol. 799). Elsevier B.V.
962 https://doi.org/10.1016/j.scitotenv.2021.149447

963 Alves, F., Pinheiro, L. M., Bueno, C., Agostini, V. O., Perez, L., Fernandes, L,
964 Weschenfelder, J., Leonhardt, A., Domingues, M., Pinho, G. L. L., Garcia-
965 Rodriguez, F., 2022. The Use of Microplastics as a Reliable Chronological

Marker of the Anthropocene Onset in Southeastern South America. SSRN Electronic Journal, 857(October 2022, 159633. https://doi.org/10.2139/ssrn.4209135.

Atwood, E. C., Falcieri, F. M., Piehl, S., Bochow, M., Matthies, M., Franke, J., Carniel, S., Sclavo, M., Laforsch, C., & Siegert, F. 2019. Coastal accumulation of microplastic particles emitted from the Po River, Northern Italy: Comparing remote sensing and hydrodynamic modelling with in situ sample collections. Marine Pollution Bulletin, 138, 561–574. https://doi.org/10.1016/j.marpolbul.2018.11.045

Baptista Neto, J. A., Gaylarde, C., Beech, I., Bastos, A. C., da Silva Quaresma, V., & de Carvalho, D. G., 2019. Microplastics and attached microorganisms in sediments of the Vitória bay estuarine system in SE Brazil. Ocean & Coastal Management, 169, 247–253. https://doi.org/10.1016/J.OCECOAMAN.2018.12.030

Barreiro, M., 2010. Influence of ENSO and the South Atlantic Ocean on climate predictability over Southeastern South America. Climate Dynamics, 35(7), 1493–1508. https://doi.org/10.1007/s00382-009-0666-9

Baudena, A., Kiko, R., Jal, I., & Pedrotti, M. L., 2023. Low-Density Plastic Debris Dispersion beneath the Mediterranean Sea Low-density plastic debris dispersion beneath the Mediterranean Sea surface. May. https://doi.org/10.1021/acs.est.2c08873

Baudena, A., Ser-Giacomi, E., Jalón-Rojas, I., Galgani, F., & Pedrotti, M. L., 2022. The streaming of plastic in the Mediterranean Sea. Nature Communications, 13(1), 2981. https://doi.org/10.1038/s41467-022-30572-5

Bertoldi, C., Lara, L. Z., Mizushima, F. A. d. L., Martins, F. C. G., Battisti, M. A., Hinrichs, R., & Fernandes, A. N., 2021. First evidence of microplastic contamination in the freshwater of Lake Guaíba, Porto Alegre, Brazil. Science of the Total Environment, 759. https://doi.org/10.1016/j.scitotenv.2020.143503

Bitencourt, L. P., Fernandes, E. H., da Silva, P. D., & Möller, O., 2020a. Spatio-temporal variability of suspended sediment concentrations in a shallow and turbid lagoon. Journal of Marine Systems, 212(April). https://doi.org/10.1016/j.jmarsys.2020.103454

997 Bitencourt, L. P., Fernandes, E., Möller, O., & Ross, L., 2020b. The contribution of ENSO
998 cycles to the salinity spatio-temporal variability in a bar-built microtidal estuary.
999 Regional Studies in Marine Science, 40, 101496.
1000 https://doi.org/10.1016/j.rsma.2020.101496

1001 Bjerknes, J., 1969. Monthly Weather Review Atmospheric Teleconnections From the
1002 Equatorial Pacific. Monthly Weather Review, 97(3), 163–172.
1003 http://journals.ametsoc.org/doi/abs/10.1175/1520-
1004 0493(1969)097%3C0163:ATFTEP%3E2.3.CO;2

1005 Bogdanowicz, A., Zubrowska-Sudol, M., Krasinski, A., & Sudol, M., 2021. Cross-
1006 contamination as a problem in collection and analysis of environmental samples
1007 containing microplastics—a review. In Sustainability (Switzerland) (Vol. 13,
1008 Issue 21). MDPI. https://doi.org/10.3390/su132112123

1009 Bogucki, D. J., Jones, B. H., & Carr, M. E., 2005. Remote measurements of horizontal
1010 eddy diffusivity. Journal of Atmospheric and Oceanic Technology, 22(9), 1373–
1011 1380. https://doi.org/10.1175/JTECH1794.1

1012 Bortolin, E. C., Távora, J., & Fernandes, E. H. L., 2022. Long-Term Variability on
1013 Suspended Particulate Matter Loads From the Tributaries of the World's Largest
1014 Choked Lagoon. Frontiers in Marine Science, 9(March), 1–17.
1015 https://doi.org/10.3389/fmars.2022.836739

1016 Boucher, J., and Friot, D., 2017. Primary Microplastics in the Oceans: a Global
1017 Evaluation of Sources. Gland: IUCN.
1018 https://doi.org/10.2305/IUCN.CH.2017.01.en

1019 Boucher, J., Faure, F., Pompini, O., Plummer, Z., Wieser, O., & de Alencastro, L. F.,
1020 2019. (Micro) plastic fluxes and stocks in Lake Geneva basin. TrAC Trends in
1021 Analytical Chemistry, 112, 66–74.
1022 https://doi.org/https://doi.org/10.1016/j.trac.2018.11.037

1023 Boucher, J., Billard, G., Simeone, E., & Sousa, J. 2020. The marine plastic footprint. In
1024 The marine plastic footprint. https://doi.org/10.2305/iucn.ch.2020.01.en

1025 Brentano, R., & Petry, M. V., 2020. Marine debris ingestion and human impacts on the
1026 Pygmy sperm whale (Kogia breviceps) in southern Brazil. Marine Pollution

Bulletin, 150(June 2019), 110595. https://doi.org/10.1016/j.marpolbul.2019.110595

Bugoni, L., Krause, L., & Petry, M. V., 2001. Marine debris and human impacts on sea turtles in Southern Brazil. Marine Pollution Bulletin, 42(12), 1330–1334. https://doi.org/10.1016/S0025-326X(01)00147-3

Calliari, L. J., Winterwerp, J. C., Fernandes, E., Cuchiara, D., Vinzon, S. B., Sperle, M., & Holland, K. T., 2009. Fine grain sediment transport and deposition in the Patos Lagoon-Cassino beach sedimentary system. Continental Shelf Research, 29(3), 515–529. https://doi.org/10.1016/j.csr.2008.09.019

Chamas, A., Moon, H., Zheng, J., Qiu, Y., Tabassum, T., Jang, J. H., Abu-Omar, M., Scott, S. L., & Suh, S., 2020. Degradation Rates of Plastics in the Environment. ACS Sustainable Chemistry and Engineering, 8(9), 3494–3511. https://doi.org/10.1021/acssuschemeng.9b06635

Cheng, Z., Jalon-Rójas, I., Wang, X. H., & Liu, Y., 2020. Impacts of land reclamation on sediment transport and sedimentary environment in a macro-tidal estuary. Estuarine, Coastal and Shelf Science, 242(October 2019). https://doi.org/10.1016/j.ecss.2020.106861

Colabuono, F. I., Barquete, V., Domingues, B. S., & Montone, R. C., 2009. Plastic ingestion by Procellariiformes in Southern Brazil. Marine Pollution Bulletin, 58(1), 93–96. https://doi.org/10.1016/j.marpolbul.2008.08.020

Cowger W, Steinmetz Z, Gray A, Munno K, Lynch J, Hapich H, Primpke S, De Frond H, Rochman C, Herodotou O., 2021. Microplastic Spectral Classification Needs an Open Source Community: Open Specy to the Rescue!. Analytical Chemistry, 93(21), 7543–7548. doi: 10.1021/acs.analchem.1c00123

Critchell, K., & Lambrechts, J., 2016. Modelling accumulation of marine plastics in the coastal zone; what are the dominant physical processes? Estuarine, Coastal and Shelf Science, 171, 111–122. https://doi.org/10.1016/j.ecss.2016.01.036

de Ramos, B., Alencar, M. V., Rodrigues, F. L., Lacerda, A. L. de F., & Proietti, M. C., 2021. Spatio-temporal characterization of litter at a touristic sandy beach in South Brazil. Environmental Pollution, 280. https://doi.org/10.1016/j.envpol.2021.116927

Defontaine, S., & Jalón-Rojas, I., 2023. Physical processes matters! Recommendations for sampling microplastics in estuarine waters based on hydrodynamics. Marine Pollution Bulletin, 191(February). https://doi.org/10.1016/j.marpolbul.2023.114932

Denuncio, P., Mandiola, M. A., Pérez Salles, S. B., Machado, R., Ott, P. H., De Oliveira, L. R., & Rodriguez, D., 2017. Marine debris ingestion by the South American Fur Seal from the Southwest Atlantic Ocean. Marine Pollution Bulletin, 122(1–2), 420–425. https://doi.org/10.1016/j.marpolbul.2017.07.013

Diez, M., Bezerra, M. O., Mosso, C., Castilla, R., & Redondo, J. M., 2008. Experimental measurements and diffusion in harbor and coastal zones. Nuovo Cimento Della Societa Italiana Di Fisica C, 31(5–6), 843–859. https://doi.org/10.1393/ncc/i2009-10354-3

dos Santos, Í. E., Fernandes, E. H. L., Pinho, G. L. L., & Abdallah, P. R., 2023. Characteristics and fluxes of plastic debris based on socio-economic data for Patos Lagoon—a choked coastal Lagoon in South Brazil. Environmental Science and Pollution Research, 30(21), 59382–59400. https://doi.org/10.1007/s11356-023-26660-8

Doyle, M., & Gilfillan, L. R., 2016. Occurrence of plastic micro-debris in the southern California Current system. August.

Fernandes, E. H., 2001. Modelling the Hydrodynamics of the Patos Lagoon, Brazil. October, 219.

Fernandes, E. H. L., Dyer, K. R., Moller, O. O., & Niencheski, L. F. H., 2002. The Patos Lagoon hydrodynamics during an El Niño event (1998). Continental Shelf Research, 22(11–13), 1699–1713. https://doi.org/10.1016/S0278-4343(02)00033-X

Fernandes, E. H. L., Mariño-Tapia, I., Dyer, K. R., & Möller, O. O., 2004. The attenuation of tidal and subtidal oscillations in the Patos Lagoon estuary. Ocean Dynamics, 54(3–4), 348–359. https://doi.org/10.1007/s10236-004-0090-y

Fernandes, E. H. L., Dyer, K. R., & Moller, O. O., 2005. Spatial gradients in the flow of Southern Patos Lagoon. Journal of Coastal Research, 21(4), 759–769. https://doi.org/10.2112/006-NIS.1

Fernandes, E. H. L., Monteiro, I. O., & Möller, O. O., 2007. On the Dynamics of Mangueira Bay—Patos Lagoon (Brazil). Journal of Coastal Research, 10047(Figure 1), 97–107. https://doi.org/10.2112/1551-5036-47.sp1.97

Fernandes, E. H. L., Da Silva, P. D., Gonçalv, G. A., & Olinto Möller, O., 2021. Dispersion plumes in open ocean disposal sites of dredged sediment. Water (Switzerland), 13(6), 1–20. https://doi.org/10.3390/w13060808

Franzen, M. O., Silva, P., Siegle, E., Fernandes, E. H. L., 2023. Influence of long jetties on estuarine and coastal hydrodynamics in a microtidal estuary. Regional Studies in Marine Science 59, 102809. https://doi.org/10.1016/j.rsma.2022.102809.

Galgani, L., & Loiselle, S. A., 2021. Plastic pollution impacts on marine carbon biogeochemistry. Environmental Pollution, 268. https://doi.org/10.1016/j.envpol.2020.115598

Geyer, R., Jambeck, J. R., & Law, K. L., 2017. Production, use, and fate of all plastics ever made. Science Advances, 3(7), 3–8. https://doi.org/10.1126/sciadv.1700782

Gorman, D., Gutiérrez, A. R., Turra, A., Manzano, A. B., Balthazar-Silva, D., Oliveira, N. R., & Harari, J., 2020. Predicting the Dispersal and Accumulation of Microplastic Pellets Within the Estuarine and Coastal Waters of South-Eastern Brazil Using Integrated Rainfall Data and Lagrangian Particle Tracking Models. Frontiers in Environmental Science, 8(October), 1–12. https://doi.org/10.3389/fenvs.2020.559405

Hardesty, B. D., Harari, J., Isobe, A., Lebreton, L., Maximenko, N., Potemra, J., van Sebille, E., Vethaak, a. D., & Wilcox, C., 2017. Using Numerical Model Simulations to Improve the Understanding of Micro-plastic Distribution and Pathways in the Marine Environment. Frontiers in Marine Science, 4(January). https://doi.org/10.3389/fmars.2017.00030

Hervouet, J.M., 2007. Hydrodynamics of Free Surface Flows: Modelling with the Finite Element Method. DOI: 10.1002/9780470319628

Jalón-rojas, I., & Marieu, V., 2023. TrackMPD A 3D numerical model to Track Marine Plastic Debris TUTORIAL.

Jalón-Rojas, I., Romero-Ramírez, A., Fauquembergue, K., Rossignol, L., Cachot, J., Sous, D., Morin, B., 2022. Effects of Biofilms and Particle Physical Properties on the Rising and Settling Velocities of Microplastic Fibers and Sheets. Environmental Science and Technology 56 (12), 8114–8123. https://doi.org/10.1021/acs.est.2c01302.

Jalón-Rojas, I., Wang, X. H., & Fredj, E., 2019. A 3D numerical model to Track Marine Plastic Debris (TrackMPD): Sensitivity of microplastic trajectories and fates to particle dynamical properties and physical processes. Marine Pollution Bulletin, 141(February), 256–272. https://doi.org/10.1016/j.marpolbul.2019.02.052

Jambeck, J. R., Geyer, R., Wilcox, C., Siegler, T. R., Perryman, M., Andrady, A., Narayan, R., & Law, K. L., 2015. Plastic waste inputs from land into the ocean. Science, 347(6223), 768–771. https://doi.org/10.1126/science.1260352

Jung, B. M., Fernandes, E. H., Möller, O. O., & García-Rodríguez, F., 2020. Estimating suspended sediment concentrations from river discharge data for reconstructing gaps of information of long-term variability studies. Water (Switzerland), 12(9), 1–14. https://doi.org/10.3390/W12092382

Kim, B. K., Hwang, J. H., & Kim, S. K., 2023. Modeling of microplastics discharged from a station in Marian Cove, West Antarctica. Marine Pollution Bulletin, 186(December 2022), 114441. https://doi.org/10.1016/j.marpolbul.2022.114441

Lacerda, A. L. d. F., Taylor, J. D., Rodrigues, L. d. S., Kessler, F., Secchi, E., & Proietti, M. C., 2022. Floating plastics and their associated biota in the Western South Atlantic. Science of the Total Environment, 805(September), 150186. https://doi.org/10.1016/j.scitotenv.2021.150186

Lemos, V. M., Lanari, M., Copertino, M., Secchi, E. R., De Abreu, P. C. O. V., Muelbert, J. H., Garcia, A. M., Dumont, F. C., Muxagata, E., Vieira, J. P., Colling, A., & Odebrecht, C., 2022. Patos Lagoon estuary and adjacent marine coastal biodiversity long-term data. Earth System Science Data, 14(3), 1015–1041. https://doi.org/10.5194/essd-14-1015-2022

Liao, F., Wang, X. H., & Fredj, E., 2023. Forecasting marine debris spill accumulation patterns in the south-eastern Australia water: an intercomparison between global

ocean forecast models. Ocean Dynamics, 73(2), 91–106. https://doi.org/10.1007/s10236-023-01539-x

Lima, C. D. M., Melo Júnior, M., Schwamborn, S. H. L., Kessler, F., Oliveira, L. A., Ferreira, B. P., Mugrabe, G., Frias, J., & Neumann-Leitão, S., 2023. Zooplankton exposure to microplastic contamination in a estuarine plume-influenced region, in Northeast Brazil. Environmental Pollution, 322 (October 2022). https://doi.org/10.1016/j.envpol.2023.121072

Lisboa, P. V., Fernandes, E. H., Sottolichio, A., Huybrechts, N., & Bendô, A. R., 2022. Coastal plumes contribution to the suspended sediment transport in the Southwest Atlantic inner continental shelf. Journal of Marine Systems, 236 (February 2021). https://doi.org/10.1016/j.jmarsys.2022.103796

López, A. G., Najjar, R. G., Friedrichs, M. A. M., Hickner, M. A., & Wardrop, D. H., 2021. Estuaries as Filters for Riverine Microplastics: Simulations in a Large, Coastal-Plain Estuary. Frontiers in Marine Science, 8(August), 1–18. https://doi.org/10.3389/fmars.2021.715924

Lozoya, J. P., Carranza, A., Lenzi, J., Machín, E., Mello, F. T. De, González, S., Hernández, D., Lacerot, G., Martínez, G., Scarabino, F., Sciandro, J., Vélez-Rubio, G., Burgues, F., Carrizo, D., Cedrés, F., Chocca, J., Álava, D. De, Jiménez, S., Leoni, V., Weisntein, F., 2015. Management and research on plastic debris in Uruguayan Aquatic Systems: update and perspectives. Revista de Gestão Costeira Integrada, May. https://doi.org/10.5894/rgci583

Marques, W. C., Fernandes, E. H., Monteiro, I. O., & Möller, O. O., 2009. Numerical modeling of the Patos Lagoon coastal plume, Brazil. Continental Shelf Research, 29(3), 556–571. https://doi.org/10.1016/j.csr.2008.09.022

Marques, W. C., Fernandes, E. H. L., & Moller, O. O., 2010a. Straining and advection contributions to the mixing process of the Patos Lagoon coastal plume, Brazil. Journal of Geophysical Research: Oceans, 115(6), 1–23. https://doi.org/10.1029/2009JC005653

Marques, W. C., Fernandes, E. H. L., Moraes, B. C., Möller, O. O., & Malcherek, A., 2010b. Dynamics of the Patos Lagoon coastal plume and its contribution to the

deposition pattern of the southern Brazilian inner shelf. Journal of Geophysical Research: Oceans, 115(10), 1–22. https://doi.org/10.1029/2010JC006190

Marques, W. C., Fernandes, E. H. L., & Rocha, L. A. O., 2011. Straining and advection contributions to the mixing process in the Patos Lagoon estuary, Brazil. Journal of Geophysical Research: Oceans, 116(3), 1–11. https://doi.org/10.1029/2010JC006524

Meijer, L. J. J., van Emmerik, T., van der Ent, R., Schmidt, C., & Lebreton, L., 2021. More than 1000 rivers account for 80% of global riverine plastic emissions into the ocean. Science Advances, 7(18), 1–14. https://doi.org/10.1126/sciadv.aaz5803

Mendrik, F., Fernández, R., Hackney, C. R., Waller, C., & Parsons, D. R., 2023. Non-buoyant microplastic settling velocity varies with biofilm growth and ambient water salinity. Communications Earth and Environment, 4(1), 1–9. https://doi.org/10.1038/s43247-023-00690-z

Moller, O. O., Castaing, P., Salomon, J. C., & Lazure, P., 2001. The influence of local and non-local forcing effects on the subtidal circulation of Patos Lagoon. Estuaries, 24(2), 297–311. https://doi.org/10.2307/1352953

Monteiro, I. O., Marques, W. C., Fernandes, E. H., Gonçalves, R. C., & Möller, O. O., 2011. On the effect of earth rotation, river discharge, tidal oscillations, and wind in the dynamics of the Patos Lagoon coastal plume. Journal of Coastal Research, 27(1), 120–130. https://doi.org/10.2112/JCOASTRES-D-09-00168.1

Morishige, C., Donohue, M. J., Flint, E., Swenson, C., & Woolaway, C., 2007. Factors affecting marine debris deposition at French Frigate Shoals, Northwestern Hawaiian Islands Marine National Monument, 1990-2006. Marine Pollution Bulletin, 54(8), 1162–1169. https://doi.org/10.1016/j.marpolbul.2007.04.014

Napper, I.E., Thompson, R.C., 2016. Release of synthetic microplastic plastic fibres from do- mestic washing machines: effects of fabric type and washing conditions. Mar. Pollut. Bull. 112 (1–2). https://doi.org/10.1016/j.marpolbul.2016.09.025

Nguyen, T. H., Kieu-Le, T. C., Tang, F. H. M., & Maggi, F., 2022. Controlling factors of microplastic fibre settling through a water column. Science of the Total

Environment, 838 (December 2021), 156011. https://doi.org/10.1016/j.scitotenv.2022.156011

Oliveira, H., Fernandes, E., Junior, O., & COLLARES, G., 2015. Processos Hidrológicos e Hidrodinâmicos da Lagoa Mirim. Revista Brasileira de Recursos Hídricos, 20(1), 34–45. https://doi.org/10.21168/rbrh.v20n1.p34-45

Pasquier, G., Doyen, P., Kazour, M., Dehaut, A., Diop, M., Duflos, G., & Amara, R., 2022. Manta Net: The Golden Method for Sampling Surface Water Microplastics in Aquatic Environments. Frontiers in Environmental Science, 10(April), 1–12. https://doi.org/10.3389/fenvs.2022.811112

Pazos, R. S., Amalvy, J., Cochero, J., Pecile, A., & Gómez, N., 2021. Temporal patterns in the abundance, type and composition of microplastics on the coast of the Río de la Plata estuary. Marine Pollution Bulletin, 168. https://doi.org/10.1016/j.marpolbul.2021.112382

Pfeiffer, F., & Fischer, E. K., 2020. Various Digestion Protocols Within Microplastic Sample Processing—Evaluating the Resistance of Different Synthetic Polymers and the Efficiency of Biogenic Organic Matter Destruction. Frontiers in Environmental Science, 8. https://doi.org/10.3389/fenvs.2020.572424

Pinheiro, L. M., Agostini, V. O., Lima, A. R. A., Ward, R. D., & Pinho, G. L. L., 2021. The fate of plastic litter within estuarine compartments: An overview of current knowledge for the transboundary issue to guide future. Environmental Pollution, 279, 116908. https://doi.org/10.1016/j.envpol.2021.116908

Pinheiro, L. M., Carvalho, I. V, Agostini, V. O., Martinez-Souza, G., Galloway, T. S., & Pinho, G. L. L., 2021. Litter contamination at a salt marsh: An ecological niche for biofouling in South Brazil. Environmental Pollution, 285(October 2020), 117647. https://doi.org/10.1016/j.envpol.2021.117647

Pritchard, M., 2000. Dynamics of a small tidal Estuarine plume. PhD Thesis. University of Plymouth, Institute of Marine Studies Faculty of Science, Plymouth, United Kingdom, unpublished

Queiroz, A. F. dos S., da Conceição, A. S., Chelazzi, D., Rollnic, M., Cincinelli, A., Giarrizzo, T., & Martinelli Filho, J. E., 2022. First assessment of microplastic and artificial microfiber contamination in surface waters of the Amazon Continental

Shelf. Science of the Total Environment, 839(March). https://doi.org/10.1016/j.scitotenv.2022.156259

Rehbein, A., & Ambrizzi, T., 2022. ENSO teleconnections pathways in South America. Climate Dynamics, December. https://doi.org/10.1007/s00382-022-06624-3

Rizzi, M., Rodrigues, F. L., Medeiros, L., Ortega, I., Rodrigues, L., Monteiro, D. S., Kessler, F., & Proietti, M. C., 2019. Ingestion of plastic marine litter by sea turtles in southern Brazil: abundance, characteristics and potential selectivity. Marine Pollution Bulletin, 140(January), 536–548. https://doi.org/10.1016/j.marpolbul.2019.01.054

Rodríguez, C., Fossatti, M., Carrizo, D., Sánchez-García, L., Teixeira de Mello, F., Weinstein, F., & Lozoya, J. P., 2020. Mesoplastics and large microplastics along a use gradient on the Uruguay Atlantic coast: Types, sources, fates, and chemical loads. Science of the Total Environment, 721. https://doi.org/10.1016/j.scitotenv.2020.137734

Schicchi, A., Moreira, D., Eisenberg, P., & Simionato, C. G. 2023. Qualitative Study of the Transport of Microplastics in the Río de la Plata Estuary, Argentina, through Numerical Simulation. Journal of Marine Science and Engineering, 11(12). https://doi.org/10.3390/jmse11122317

Schossler, V., Simões, J. C., Aquino, F. E., & Viana, D. R., 2018. Precipitation anomalies in the brazilian southern coast related to the SAM and ENSO climate variability modes. Revista Brasileira de Recursos Hidricos, 23. https://doi.org/10.1590/2318-0331.231820170081

Schossler, V., Simões, J. C., Aquino, F. E., & Viana, D. R., 2018. Precipitation anomalies in the brazilian southern coast related to the SAM and ENSO climate variability modes. Revista Brasileira de Recursos Hidricos, 23. https://doi.org/10.1590/2318-0331.231820170081

Tavora, J., Fernandes, E. H. L., Thomas, A. C., Weatherbee, R., & Schettini, C. A. F., 2019. The influence of river discharge and wind on Patos Lagoon, Brazil, Suspended Particulate Matter. International Journal of Remote Sensing, 40(12), 4506–4525. https://doi.org/10.1080/01431161.2019.1569279

Uzun, P., Farazande, S., & Guven, B., 2022. Mathematical modeling of microplastic abundance, distribution, and transport in water environments: A review. In Chemosphere (Vol. 288). Elsevier Ltd. https://doi.org/10.1016/j.chemosphere.2021.132517

van Emmerik, T. H. M., Frings, R. M., Schreyers, L. J., Hauk, R., de Lange, S. I., & Mellink, Y. A. M., 2023a. River plastic transport and deposition amplified by extreme flood. Nature Water, 1(6), 514–522. https://doi.org/10.1038/s44221-023-00092-7

van Emmerik, T., Kirschke, S., Nath, S., Schmidt, C., Wendt-Potthoff, K., & van Emmerik, T. H., 2023b. Estimating plastic pollution levels in rivers through harmonized monitoring strategies. Springer Nature (Paper Still under Review), 196(October), 0–21. https://doi.org/10.1016/j.marpolbul.2023.115503

Verma, R., Vinoda, K. S., Papireddy, M., & Gowda, A. N. S. (2016). Toxic Pollutants from Plastic Waste- A Review. Procedia Environmental Sciences, 35, 701–708. https://doi.org/10.1016/j.proenv.2016.07.069

Villaret, C., Hervouet, J.M., Kopmann, R., Merkel, U., Davies, A.G., 2013. Morpho-dynamic modeling using the Telemac finite-element system. Comput. Geosci. 53, 105–113.

Wang, T., Zhao, S., Zhu, L., Mcwilliams, J. C., & Galgani, L., 2022. Accumulation, transformation and transport of microplastics in estuarine fronts. 3(November), 795–805. https://doi.org/10.1038/s43017-022-00349-x

Wetzel, L., Fillmann, G., Niencheski, L.F.H., 2004. Litter contamination processes and management perspectives on the southern brazilian coast. Int. J. Environ. Pollut. 21 (2), 153–165. https://doi.org/10.1504/IJEP.2004.004182

Zamora, A. M., Caterbow, A., Nobre, C. R., Duran, C., Muffett, C., Flood, C., Rehmer, C., Chemnitz, C., Lauwigi, C., Arkin, C., Costa, C. da, Bispo, D., Amorim, D., Azoulay, D., Knoblauch, D., Seeger, D., Moun, D., Silveira, I. da, Patton, J., … Feit, S., 2020. Atlas do plástico - Fatos e números sobre o mundo dos polímeros sintéticos. Fundação Heinrich Böll, 01, 64. https://br.boell.org/pt-br/2020/11/29/atlas-do-plastico

Zavialov, P. O., Moller Jr., O. O., & Wang, X. H., 2020. Relations between marine plastic litter and river plumes: First results of PLUMPLAS project. Journal of Oceanological Research, 48(4), 32–44. https://doi.org/10.29006/1564-2291.JOR-2020.48(4).2

Zhao, S., Wang, T., Zhu, L., Xu, P., Wang, X., Gao, L., & Li, D., 2019. Analysis of suspended microplastics in the Changjiang Estuary: Implications for riverine plastic load to the ocean. Water Research, 161, 560–569. https://doi.org/10.1016/j.watres.2019.06.019

Zheng, Y., Li, J., Sun, C., Cao, W., Wang, M., Jiang, F., & Ju, P., 2021. Comparative study of three sampling methods for microplastics analysis in seawater. Science of the Total Environment, 765. https://doi.org/10.1016/j.scitotenv.2020.144495

Kjerfve, B. 1986. Comparative Oceanography of Coastal Lagoons. Estuarine Variability, December 1986, 63–81. https://doi.org/10.1016/b978-0-12-761890-6.50009-5